Inorganic Chemistry

Article

pubs.acs.org/IC

Sensitivity of a Strained C−C Single Bond to Charge Transfer: Redox Activity in Mononuclear and Dinuclear Ruthenium Complexes of Bis(arylimino)acenaphthene (BIAN) Ligands

Prasenjit Mondal,[†] Hemlata Agarwala,[†] Rahul Dev Jana,[†] Sebastian Plebst,[‡] Anita Grupp,[‡] Fabian Ehret,[‡] Shaikh M. Mobin,[§] Wolfgang Kaim,*[,‡] and Goutam Kumar Lahiri*[,†]

[†]Department of Chemistry, Indian Institute of Technology Bombay, Powai, Mumbai 400076, India

[‡]Institut für Anorganische Chemie, Universität Stuttgart, Pfaffenwaldring 55, D-70550 Stuttgart, Germany

[§]Discipline of Chemistry, School of Basic Sciences, Indian Institute of Technology Indore, Indore 452017, India

Supporting Information

ABSTRACT: The new compounds $[Ru(acac)_2(BIAN)]$, BIAN = bis(arylimino)-acenaphthene (aryl = Ph (**1a**), 4-MeC_6H_4 (**2a**), 4-$OMeC_6H_4$ (**3a**), 4-ClC_6H_4 (**4a**), 4-$NO_2C_6H_4$ (**5a**)), were synthesized and structurally, electrochemically, spectroscopically, and computationally characterized. The α-diimine sections of the compounds exhibit intrachelate ring bond lengths 1.304 Å < d(CN) < 1.334 and 1.425 Å < d(CC) < 1.449 Å, which indicate considerable metal-to-ligand charge transfer in the ground state, approaching a $Ru^{III}(BIAN^{\bullet-})$ oxidation state formulation. The particular structural sensitivity of the strained peri-connecting C−C bond in the BIAN ligands toward metal-to-ligand charge transfer is discussed. Oxidation of $[Ru(acac)_2(BIAN)]$ produces electron paramagnetic resonance (EPR) and UV−vis−NIR (NIR = near infrared) spectroelectrochemically detectable Ru^{III} species, while the reduction yields predominantly BIAN-based spin, in agreement with density functional theory (DFT) spin-density calculations. Variation of the substituents from CH_3 to NO_2 has little effect on the spin distribution but affects the absorption spectra. The dinuclear compounds $\{(\mu\text{-tppz})[Ru(Cl)(BIAN)]_2\}(ClO_4)_2$, tppz = 2,3,5,6-tetrakis(2-pyridyl)pyrazine; aryl (BIAN) = Ph ($[\mathbf{1b}](ClO_4)_2$), 4-MeC_6H_4 ($[\mathbf{2b}](ClO_4)_2$), 4-$OMeC_6H_4$ ($[\mathbf{3b}](ClO_4)_2$), 4-ClC_6H_4 ($[\mathbf{4b}](ClO_4)_2$), were also obtained and investigated. The structure determination of $[\mathbf{2b}](ClO_4)_2$ and $[\mathbf{3b}](ClO_4)_2$ reveals *trans* configuration of the chloride ligands and unreduced BIAN ligands. The DFT and spectroelectrochemical results (UV−vis−NIR, EPR) indicate oxidation to a weakly coupled $Ru^{III}Ru^{II}$ mixed-valent species but reduction to a tppz-centered radical state. The effect of the π electron-accepting BIAN ancillary ligands is to diminish the metal−metal interaction due to competition with the acceptor bridge tppz.

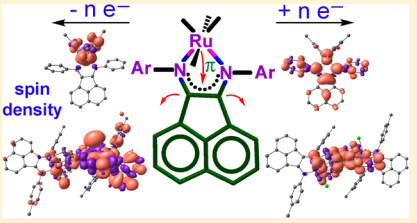

INTRODUCTION

The bis(arylimino)acenaphthene (BIAN) ligands are members of the α-diimine class of chelate ligands, which have been employed in catalysis and other studies.[1−7] In addition to the preformed *cis* structure of the metal coordinating imine functions for chelation, these ligands have received attention due to their electronic structure, which can be described as involving a combination of the α-diimine section with a naphthalene part.[2,4]

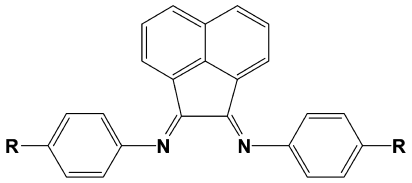

BIAN

R = H, Me, OMe, Cl, NO_2

Ligands that are made up of conjugated coordination functions and mainly electron transfer-active regions, such as 1,10-phenanthroline (phen),[8] dipyrido[3,2-*a*:2′,3′-*c*]phenazine (dppz),[9] 2,3-bis(1-methylimidazol-2-yl)quinoxaline (bmiq),[10] or 3,6-bis(4-pyridyl)-1,2,4,5-tetrazine (4,4′-bptz),[11] have long been the subject of experimental and molecular orbital analysis. The presence of two low-lying unoccupied molecular orbitals, namely, $\pi^*(\alpha\text{-diimine})$ ($\mathbf{5b}_2$) and π^*(naphthalene) ($\mathbf{4a}_2$), in BIAN systems raises the question as to how many electrons this ligand can accept from a coordinated metal. Electron paramagnetic resonance (EPR) and structure-based reports have revealed that 1,2-bis[(2,6-diisopropylphenyl)imino]-acenaphthene can be reduced stepwise to a tetraanion,[4a] with the first two electrons added to the α-diimine part and the last two electrons delocalized over the whole, multiply cation-coordinated π system.

To probe whether the BIAN ligands can accept as many as four electrons[2] and to extend the potential of the BIAN ligands, we describe here two kinds of ruthenium complexes (Scheme 1). The $Ru(acac)_2$ complex fragment as present in **1a**−**5a** is

Received: March 28, 2014
Published: July 1, 2014

   dx.doi.org/10.1021/ic500730m | *Inorg. Chem.* 2014, 53, 7389−7403

Scheme 1. Representation of Complexes Studied

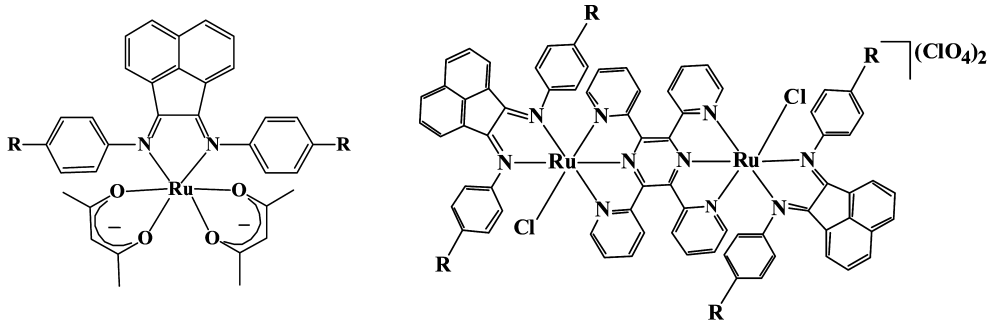

R= H(**1a**), Me(**2a**), OMe(**3a**), Cl(**4a**), NO_2(**5a**)

R= H([**1b**]$(ClO)_2$), Me([**2b**]$(ClO)_2$), OMe([**3b**]$(ClO)_2$), Cl([**4b**]$(ClO)_2$)

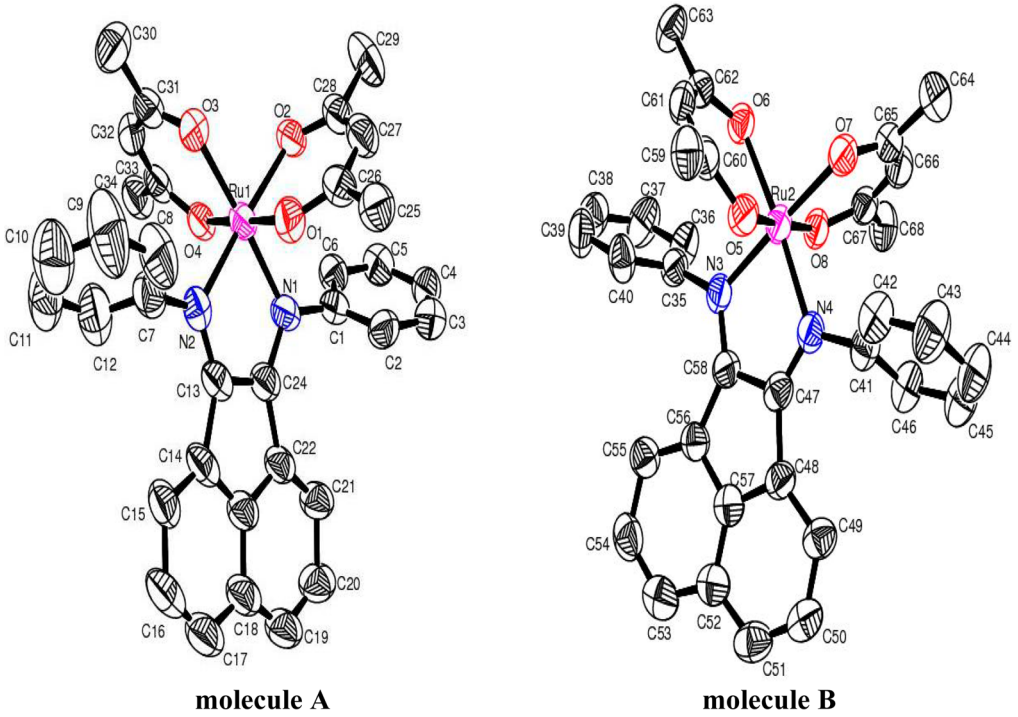

molecule A **molecule B**

Figure 1. ORTEP diagram of **1a.** Ellipsoids are drawn at the 50% probability level. Hydrogen atoms are omitted for clarity.

known to be a strong π donor, often transferring electrons to acceptor ligands while undergoing oxidation to the Ru^{III} or even Ru^{IV} state.[12] On the other hand, the 2,3,5,6-tetrakis(2-pyridyl)pyrazine (tppz) bridge is a strongly π-accepting bis-tridentate ligand, which can compete with α-diimines (such as BIAN) for charge from the metal(s); it may also affect metal−metal interaction in mixed-valent situations.[13] The present study uses experimental techniques (crystal structure determination, electrochemistry, EPR, UV−vis−NIR (NIR = near infrared) spectroelectrochemistry) and computational methods in elucidating the electronic structures of the complexes and in evaluating the noninnocent ligand[14] potential of the BIAN ligands.

RESULTS AND DISCUSSION

Synthesis and Characterization. The electrically neutral diamagnetic complexes $Ru(acac)_2(BIAN)$, where $acac^-$ = acetylacetonate = 2,4-pentanedionate and BIAN = bis(arylimino)acenaphthene (aryl = Ph (**1a**), 4-MeC_6H_4 (**2a**), 4-$OMeC_6H_4$ (**3a**), 4-ClC_6H_4 (**4a**), 4-$NO_2C_6H_4$ (**5a**)), were prepared from the precursor $Ru(acac)_2(CH_3CN)_2$ and the respective BIAN ligands in refluxing ethanol under a dinitrogen atmosphere, followed by chromatographic purification on a silica gel column. The tppz-bridged diamagnetic diruthenium compounds $[(BIAN)(Cl)Ru^{II}(\mu\text{-tppz})Ru^{II}(BIAN)(Cl)](ClO_4)_2$, where BIAN (aryl = Ph ([**1b**]$(ClO_4)_2$), 4-MeC_6H_4 ([**2b**]$(ClO_4)_2$), 4-$OMeC_6H_4$ ([**3b**]$(ClO_4)_2$), 4-ClC_6H_4 ([**4b**]$(ClO_4)_2$)), were synthesized via the reactions of BIAN ligands with the precursor complex $Cl_3Ru(\mu\text{-tppz})RuCl_3$.

The compounds (**1a**−**5a** and [**1b**]$(ClO_4)_2$−[**4b**]$(ClO_4)_2$) were characterized by microanalytical, molar conductivity, mass spectrometric (Figures S13 and S20 of the Supporting Information), and IR and ^1H NMR spectroscopic data (Figures S14 and S21, Supporting Information, and Experimental Section). The diamagnetic complexes exhibit the expected number of aromatic and aliphatic (CH and CH_3) ^1H NMR resonances within the chemical shift range of 0−10 ppm. Slight variations of chemical shifts were observed, depending on the

dx.doi.org/10.1021/ic500730m | Inorg. Chem. 2014, 53, 7389−7403

Table 1. Selected Crystallographic Data for 1a, 2a, 4a, 5a, [2b](ClO$_4$)$_2$·0.5H$_2$O, and [3b](ClO$_4$)$_2$

complex	2 × **1a**	2 × **2a**	2 × **4a**	2 × **5a**	[**2b**](ClO$_4$)$_2$. 0.5H$_2$O	[**3b**](ClO$_4$)$_2$
empirical formula	$C_{68}H_{60}N_4O_8$ Ru_2	$C_{72}H_{68}N_4O_8$ Ru_2	$C_{68}H_{56}Cl_4N_4O_8$ Ru_2	$C_{68}H_{56}N_8O_{16}$ Ru_2	$C_{76}H_{56}Cl_4N_{10}O_{8.50}$ Ru_2	$C_{76}H_{56}Cl_4N_{10}O_{12}$ Ru_2
fw	1263.39	1319.44	1401.11	1443.35	1589.25	1645.25
crystal system	triclinic	triclinic	triclinic	triclinic	triclinic	monoclinic
space group	$P\bar{1}$	$P\bar{1}$	$P\bar{1}$	$P\bar{1}$	$P\bar{1}$	$C2/c$
a (Å)	11.8301(9)	11.9357(6)	11.6789(3)	11.8755(8)	14.3601(13)	30.8584(8)
b (Å)	12.5877(9)	14.0574(8)	13.8716(3)	14.1654(6)	14.8626(14)	14.7627(4)
c (Å)	20.3389(13)	20.2303(11)	20.1947(5)	20.0240(10)	16.8788(19)	14.3067(4)
α (deg)	105.246(6)	73.342(5)	107.434(2)	74.629(4)	108.718(9)	90
β (deg)	90.936(6)	89.530(4)	90.346(2)	88.123(5)	101.818(9)	99.176(2)
γ (deg)	92.430(6)	88.403(4)	90.358(2)	88.540(4)	90.234(8)	90
V (Å^3)	2918.3(4)	3250.6(3)	3121.18(13)	3245.7(3)	3330.1(6)	6434.1(3)
Z	2	2	2	2	2	4
μ (mm^{-1})	0.578	0.522	0.714	0.541	5.714	0.714
T (K)	150(2)	150(2)	150(2)	150(2)	150(2)	150(2)
D_{calcd} (g cm^{-3})	1.438	1.348	1.491	1.477	1.585	1.698
F(000)	1296	1360	1424	1472	1612	3336
θ range (deg)	3.00 to 25.00	3.03 to 25.00	2.94 to 25.00	3.12 to 25.00	3.15 to 72.93	2.99 to 25.00
data/restraints/parameters	10 237/0/747	11 420/15/787	10 974/0/783	11 404/22/855	12 687/21/914	5667/0/471
$R1$, $wR2$ [$I > 2\sigma(I)$]	0.0639, 0.1560	0.0522, 0.1238	0.0438, 0.1104	0.0798, 0.2116	0.0987, 0.2169	0.0419, 0.1061
$R1$, $wR2$ (all data)	0.0909, 0.1837	0.0664, 0.1329	0.0501, 0.1158	0.1000, 0.2308	0.1881, 0.2852	0.0530, 0.1150
GOF	1.088	1.110	1.045	1.039	1.063	1.062
largest diff. peak/hole, (e Å^{-3})	1.479/−1.182	0.806/−0.802	2.017/−2.005	2.286/−2.082	1.202/−0.790	0.913/−0.641

Table 2. Selected Experimental Bond Lengths (Å) for 1a, 2a, 4a, and 5a

	molecule A					molecule B			
bond length (Å)	**1a**	**2a**	**4a**	**5a**	bond length (Å)	**1a**	**2a**	**4a**	**5a**
Ru(1)−N(1)	1.995(5)	1.992(3)	1.995(3)	1.996(5)	Ru(2)−N(3)	1.995(4)	1.986(4)	1.994(3)	
Ru(1)−N(2)	1.980(5)	1.997(4)	2.007(3)	2.018(5)	Ru(2)−N(4)	2.009(5)	1.995(4)	1.993(3)	
Ru(1)−O(1)	2.026(4)	2.025(3)	2.048(2)	2.059(4)	Ru(2)−O(5)	2.026(3)	2.030(4)	2.044(3)	
Ru(1)−O(2)	2.038(4)	2.050(3)	2.034(3)	2.032(5)	Ru(2)−O(6)	2.048(4)	2.042(3)	2.032(3)	
Ru(1)−O(3)	2.044(4)	2.035(3)	2.054(3)	2.048(5)	Ru(2)−O(7)	2.053(4)	2.026(3)	2.040(3)	
Ru(1)−O(4)	2.020(4)	2.052(3)	2.028(2)	2.029(5)	Ru(2)−O(8)	2.027(3)	2.045(4)	2.033(3)	
N(1)−C(24)	1.329(7)	1.326(5)	1.320(5)	1.320(8)	N(3)−C(58)	1.316(7)	1.310(6)	1.309(5)	
N(2)−C(13)	1.312(7)	1.319(5)	1.310(5)	1.316(8)	N(4)−C(47)	1.303(7)	1.335(5)	1.323(5)	
C(13)−C(24)	1.430(8)	1.449(6)	1.449(5)	1.435(9)	C(47)−C(58)	1.447(8)	1.436(7)	1.439(5)	1.422(9)
					Ru(2)−N(5)				1.991(6)
					Ru(2)−N(6)				1.999(5)
					Ru(2)−O(9)				2.054(5)
					Ru(2)−O(10)				2.040(5)
					Ru(2)−O(11)				2.026(5)
					Ru(2)−O(12)				1.996(6)
					N(5)−C(58)				1.313(9)
					N(6)−C(47)				1.321(8)

electron-donating or -withdrawing effect of the substituents in the aryl rings of the BIAN ligand. The identity of the complexes was authenticated by single-crystal X-ray structures of several derivatives (**1a**, **2a**, **4a**, **5a**, [**2b**](ClO$_4$)$_2$, and [**3b**](ClO$_4$)$_2$).

Structural Investigation of [Ru(acac)$_2$(BIAN)]. The molecular structures and the selected crystallographic and structural parameters of compounds **1a**, **2a**, **4a**, and **5a** are shown in Figure 1, Figures S2−S4 (Supporting Information), Tables 1 and 2, and Tables S3−S8 (Supporting Information), respectively. In each case the asymmetric unit in the single crystal consists of two independent molecules (molecules **A** and **B**) with only slight differences in the bond parameters. The slightly distorted octahedral arrangement around the metal ions in the crystals of **1a**, **2a**, **4a**, and **5a** is evident from the angles listed in Tables S5 and S6 of the Supporting Information. The average Ru−O distance in **1a**, **2a**, **4a**, and **5a** (2.035−2.039 Å) is ∼0.01 Å longer than that reported for [Ru^{III}(acac)$_2$(Q$^{\bullet-}$)] (Q$^{\bullet-}$ = 4,6-di-*tert*-butyl-*N*-phenyl-*o*-iminobenzosemiquinone) (2.028 Å)[15] but shorter than in [Ru^{II}(acac)$_2$(Q^0)] (Q^0 = 9,10-phenanthrenequinonediimine) (2.051 Å).[16]

Since the [Ru(acac)$_2$] complex fragment is strongly π electron-donating[12] and the BIAN ligands are π accepting, the question is as to how much metal-to-ligand electron transfer can occur in the ground state. 1,4-Diazabutadiene[17] and *o*-benzoquinonediimine systems[18] with coordinated [Ru(acac)$_2$] have been reported to show very strong metal/diimine interaction. Experimental criteria for ligand oxidation states[14] have increasingly been quantified in the form of characteristic

dx.doi.org/10.1021/ic500730m | Inorg. Chem. 2014, 53, 7389−7403

"metric parameters"[19,20] from crystal-structure determinations. For the four-center π system of α-diimines it has long been established that the unreduced native state, the radical anion intermediates, and the two-electron-reduced 1,2-enediamido forms can be distinguished according to Scheme 2 with characteristically changing CN and CC bond lengths.[17,19]

Scheme 2. 1,4-Diazabutadiene/ene-1,2-diamido Two-Step Redox Series

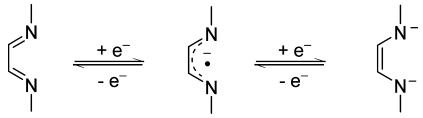

Using established metal complexes of neutral α-diimine ligands, of dianionic 1,2-ene-diamido ligands, and especially of monoanionic $(\alpha\text{-diimine})^{\bullet-}$ radical ligands with EPR-spectroscopically confirmed oxidation states as references,[17] we are led to formulate compounds **1a**−**5a** as BIAN radical anion complexes of the $[Ru(acac)_2]^+$ entity. At 1.304 Å < d(CN) < 1.334 Å and 1.425 Å < d(CC) < 1.449 Å the oxidation state-revealing intrachelate CN and CC bonds (Table 2) suggest a $Ru^{III}(L^{\bullet-})$ oxidation state formulation. Similar values were noted for complexes $[Ru(acac)_2(R{-}DAB)]$ with 1.297 Å < d(CN) < 1.344 Å and 1.382 Å < d(CC) < 1.425 Å,[17] while the structure determination for a BIAN radical anion (Na^+ salt) with d(CC) = 1.446(2) Å and d(CN) ≈ 1.33 Å[4a] confirms this assignment. In BIAN complexes $\{[ML_n](BIAN)\}$ of less π-donating metal centers the CN bonds are shorter (<1.30 Å), while the connecting CC bonds are distinctly longer at 1.473(10) Å ($ML_n = [Ir^{III}Cp^*Cl]^+$) (Cp = cyclopentadienyl),[7a] 1.49−1.50 Å (ML_n, e.g., $[Pd^{II}(MA)]$, MA = maleic anhydride,[1] or organometallic Ru^{II} [3]), and 1.521(4) Å ($[Re^{I}(CO)_3Cl]$);[21] the free ligands have d(CC) > 1.52 Å (Tables S1 and S2, Supporting Information).[22] The longer CC bonds for the BIAN complexes and their "diagnostic value"[6] result from the strain exerted by the 1,8-positioned "peri" centers to retain sp^2 hybridization, pulling the C atoms apart. Instead of 120° the external bond angles at the peri C atoms C(13)−C(14)−C(23) and C(13)−C(14)−C(15) are about 105° and 135° (Figure 1, Tables S5 and S6 of the Supporting Information, Chart1). As a result, the bond length variation between corresponding free ligands and their $[Ru(acac)_2]$ complexes is about twice as large for the BIAN systems (1.53−1.44 Å) than it is for the sterically less strained R−DAB compounds (1.45−1.40 Å).[17] A density functional theory (DFT) calculation for the neutral and anionic forms of diiminoacenaphthene yields a difference of 1.53 − 1.46 Å = 0.07 Å for that C−C bond (Table S2 and Figures S1 and S5 of the Supporting Information).

Chart 1

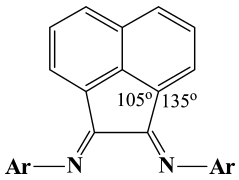

Regardless of formal oxidation state assignment, there is a considerable amount of metal-to-ligand electron transfer occurring in the ground state. The oxidation of ruthenium(II) in the precursor $[Ru(acac)_2(CH_3CN)_2]$ to a ruthenium(III) species would be accompanied by strongly antiferromagnetically coupled spins on $BIAN^{\bullet-}$ and Ru^{III}. DFT calculations (Tables S9, S12 and Figures S6, S7, Supporting Information) confirm the experimental results. In agreement with this, the diamagnetic compounds **1a**−**5a** are EPR-silent and exhibit conventional ^1H NMR resonance signals.

The ability of $[Ru(acac)_2(CH_3CN)_2]$ to reductively react with strong π-acceptor ligands has been demonstrated before in a number of reactions with α-azocarbonyl,[23] α-azothiocarbonyl,[23b] and α-azoimine ligands.[24] The enhanced π-acceptor capability of the BIAN ligands in comparison, for example, with 2,2′-bipyridine allows for extensive charge transfer in the ground state.

The structural data observed here are not only similar to the averages of 1.32/1.33 Å (d(CN)) and 1.40/1.39 Å (d(CC)) reported for $Ru(acac)_2(R{-}DAB)$,[17] but also for *cis*-$Mo(Mes{-}DAB)_2(CO)_2$ (Mes = mesityl).[25] Because of conflicting results with K-edge energy data from XAS spectroscopy it was claimed for *cis*-$Mo(Mes{-}DAB)_2(CO)_2$ that "serendipitously, the bond lengths as established by X-ray crystallography coincide exactly with the established π-radical ligand."[25] Recent[17] and present examples show that time-dependent (TD) DFT-supported spectroscopy suggests metal ligand covalency and electron delocalization in the compounds **1a**−**5a**, as further studied by (spectro)electrochemistry.

Electrochemistry and Spectroelectrochemistry of $[Ru(acac)_2(BIAN)]$. The metal−ligand mixed ground state $[Ru^{III}(BIAN)^{\bullet-}]$ can undergo electron transfer in several directions. Both the metal and the ligand radical anion can be oxidized as well as reduced, as illustrated by cyclic voltammetry (Figure 2, Table 3). All compounds **1a**−**5a** show a reversible oxidation and reduction, and the nitro-substituted compound **5a** exhibits a second reduction process within the available redox potential range. Apparently, the electronic structure is different in the case of $(\mathbf{5a})^{n-}$. The redox potentials reflect the substituent effects, exhibiting more positive values for **5a** with its accepting nitro groups.

EPR and UV−vis−NIR spectroelectrochemistry were employed to identify the site of electron transfer on oxidation and reduction. EPR spectra of the cations $\mathbf{1a}^+$, $\mathbf{2a}^+$, $\mathbf{4a}^+$, and $\mathbf{5a}^+$ were obtained in frozen solution, showing sizable splitting of the three g tensor components (Figure 3, Figures S10−S12 of the Supporting Information, and Table 4). The values and the patterns are compatible[26] with ruthenium(III) systems involving some $acac^-$ contributions but little BIAN ligand participation at the spin distribution, as confirmed by DFT calculations (Figure 4 and Table 5). The large spin−orbit coupling parameter of ruthenium (1200 cm^{-1})[27] is responsible for the g anisotropy, thus providing evidence for metal-based spin.

The EPR signals obtained after reduction to $\mathbf{1a}^-$, $\mathbf{2a}^-$, $\mathbf{4a}^-$, and $\mathbf{5a}^-$ exhibit much smaller g anisotropy in frozen acetonitrile/0.1 M Bu_4NPF_6 solution (Figure 3, Figures S10−S12 of the Supporting Information, and Table 4). In agreement with DFT calculations this supports the formulation of ruthenium(II) complexes of anion radical ligands.[17,26,27] At room temperature in CH_3CN solution the EPR spectrum is unresolved except for a $^{99,101}Ru$ isotope coupling of about 1.3 mT, a relatively high value for a radical complex (^{99}Ru: 12.7% natural abundance, I = 5/2; ^{101}Ru: 17.0%, I = 5/2).[26,27] Accordingly, Scheme 3 illustrates that the oxidation of the compounds **1a**−**5a** occurs at the $(BIAN)^{\bullet-}$ ligand, whereas the

dx.doi.org/10.1021/ic500730m | Inorg. Chem. 2014, 53, 7389−7403

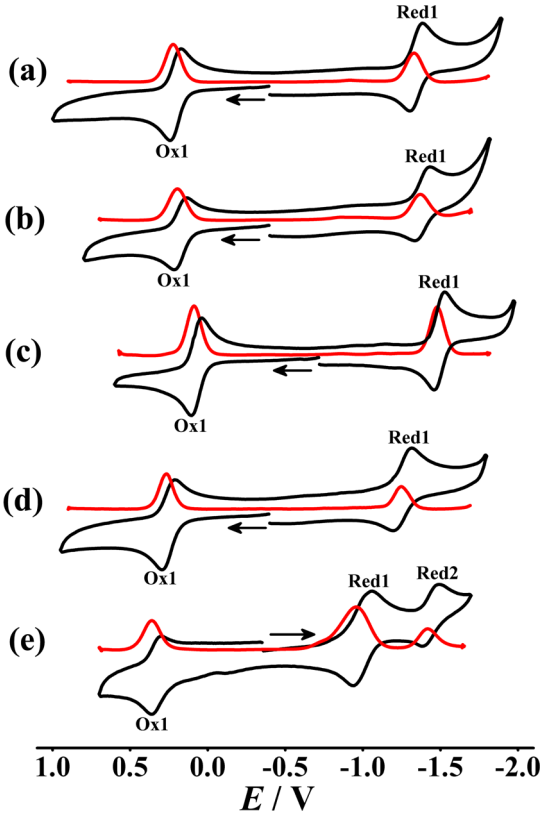

Figure 2. Cyclic voltammograms (black) and differential pulse voltammograms (red) of (a) **1a**, (b) **2a**, (c) **3a**, (d) **4a**, and (e) **5a** in CH_3CN/0.1 M NEt_4ClO_4 at 298 K. Scan rate: 100 mV s^{-1}.

reduction occurs at the metal. However, a situation with a Ru^{III} species after oxidation and an anion radical compound of ruthenium(II) after reduction would also be expected for a conventional $[Ru^{II}(\alpha\text{-diimine})]$ complex.[27] The different spin location for the oxidized and the reduced species is also illustrated by the nearly axial EPR signal for the former but a more rhombic g symmetry for the latter (Figure 3). Figure 4 depicts the metal-based spin for the cations and the ligand-centered spin for the anionic species, leading to Scheme 3 for the two-step redox series.

Considering the diagnostic value[6] of the external C−C bond as outlined above, the DFT results for $\mathbf{1a}^n$ and $\mathbf{5a}^n$ = $[Ru(acac)_2(BIAN)]^n$, n = +, 0, −, from Tables S3, S4, and S9−S15 (Supporting Information), indicate a continuous shortening of this parameter from 1.492 Å via 1.466 Å (exp: 1.448(8) Å) to 1.430 Å. This behavior agrees perfectly with the above-mentioned EPR results for cations and anions and suggests that the crystallographically characterized neutral

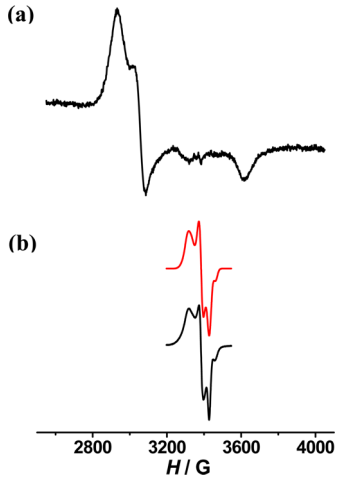

Figure 3. EPR spectra of electrogenerated (a) $\mathbf{1a}^+$ and (b) $\mathbf{1a}^-$ (black, experimental; red, simulated) in CH_3CN/0.1 M NBu_4PF_6 at 110 K.

Table 4. EPR Parameters for $\mathbf{1a}^n$, $\mathbf{2a}^n$, $\mathbf{4a}^n$, and $\mathbf{5a}^n$ from Measurements at 110 K in CH_3CN/0.1 M Bu_4NPF_6

complex	g_1	g_2	g_3	Δg^a	$\langle g\rangle^b$
$\mathbf{1a}^+$ (S = 1/2)	2.307	2.215	1.871	0.436	2.139
$\mathbf{1a}^-$ (S = 1/2)	2.041	2.001[c]	1.975[d]	0.066	2.006[e]
$\mathbf{2a}^+$ (S = 1/2)	2.292	2.211	1.876	0.416	2.134
$\mathbf{2a}^-$ (S = 1/2)	2.037	2.000	1.977	0.060	2.005
$\mathbf{4a}^+$ (S = 1/2)	2.291	2.204	1.882	0.409	2.133
$\mathbf{4a}^-$ (S = 1/2)	2.045	2.004	1.972	0.073	2.007
$\mathbf{5a}^+$ (S = 1/2)	2.284	2.197	1.879	0.405	2.127
$\mathbf{5a}^-$ (S = 1/2)	2.020	2.005	1.981	0.039	2.002

[a] $\Delta g = g_1 - g_3$. [b] $\langle g\rangle = \{(1/3)(g_1^2 + g_2^2 + g_3^2)\}^{1/2}$. [c] $A_2(^{99,101}Ru)$ = 2.85 mT. [d] $A_3(^{99,101}Ru)$ = 1.37 mT. [e] At 298 K: g = 2.0048, $A(^{99,101}Ru)$ = 1.50 mT.

forms are best described by a resonance formulation (Scheme 3), bearing in mind that the DFT approach favors delocalized situations.

Both oxidation and reduction of the systems **1a−5a** (Figure 5, Figures S8 and S9 (Supporting Information), and Table 6) cause a diminishing of the metal-to-ligand charge transfer (MLCT) absorption band at about 520 nm. Other bands emerge, involving the singly occupied molecular orbital (SOMO) as starting level of transitions or as target orbital. The MLCT absorption band of **1a−5a** is expectedly[17,19] diminished and shifted to about 650 nm on reduction to the anion radical complex. Ligand-to-ligand charge transfer (LLCT) is made responsible for the additional absorption in the NIR. On oxidation, the MLCT band is replaced by an LMCT absorption at about 550 nm. While the TD-DFT

Table 3. Electrochemical Data[a] for 1a−5a

	$E°_{298}$[V](ΔE[mV])[b]			K_c[c]	
complex	Ox1	Red1	Red2	K_{c1}[d]	K_{c2}[d]
1a	0.21 (80)	−1.34 (80)		2×10^{26}	
2a	0.17 (80)	−1.39 (80)		$2. \times 10^{26}$	
3a	0.08 (70)	−1.48 (70)		3×10^{26}	
4a	0.26 (80)	−1.25 (120)		4×10^{25}	
5a	0.33 (60)	−0.99 (120)	−1.44 (100)	2×10^{22}	4.24×10^{7}

[a] From cyclic voltammetry in CH_3CN/0.1 M Et_4NClO_4 at 100 mV s^{-1}. [b] Potential in V versus SCE; peak potential differences ΔE_p [mV] (in parentheses). [c] Comproportionation constant from RT ln $K_c = nF(\Delta E)$. [d] K_{c1} between Ox1 and Red1, K_{c2} between Red1 and Red2.

dx.doi.org/10.1021/ic500730m | Inorg. Chem. 2014, 53, 7389−7403

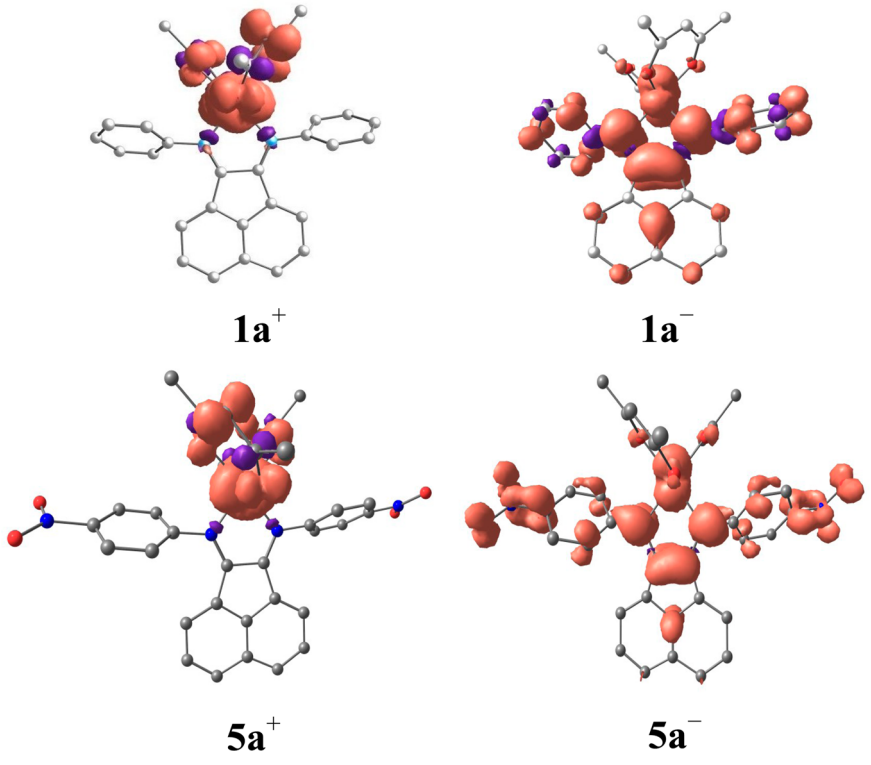

Figure 4. DFT-calculated Mulliken spin-density plots of $\mathbf{1a}^n$ and $\mathbf{5a}^n$.

Table 5. DFT-Calculated Mulliken Spin Distributions for $\mathbf{1a}^n$ and $\mathbf{5a}^n$

complex	Ru	acac	BIAN
$\mathbf{1a}^+$ (S = 1/2)	0.796	0.216	−0.012
$\mathbf{1a}^-$ (S = 1/2)	0.198	0.005	0.798
$\mathbf{5a}^+$ (S = 1/2)	0.782	0.233	−0.008
$\mathbf{5a}^-$ (S = 1/2)	0.252	0.015	0.736

Scheme 3. Assignments of Oxidation States in the Redox Series of Complexes $[Ru(acac)_2(BIAN)]^n$

$$[\mathbf{Ru^{III}(BIAN)}]^+ \text{ or } [Ru^{IV}(BIAN^{\bullet-})]^+$$
$$\overset{-e^-}{\underset{+e^-}{\rightleftharpoons}}$$
$$[\mathbf{Ru^{III}(BIAN^{\bullet-})}] \longleftrightarrow [\mathbf{Ru^{II}(BIAN)}]$$
$$\overset{-e^-}{\underset{+e^-}{\rightleftharpoons}}$$
$$[\mathbf{Ru^{II}(BIAN^{\bullet-})}] \text{ or } [Ru^{III}(BIAN^{2-})]^-$$

(dominant alternatives in boldface)

calculations (for $\mathbf{1a}^n$, see Table 7a; for $\mathbf{5a}^n$, see Table 7b) are generally reproducing the observed absorptions and may thus be used for the assignment of transitions in most cases, the nitro-substituted system $\mathbf{5a}^n$ exhibits unusually strong NIR absorptions (Figure 5), the high intensity of which could not be fully reproduced by the calculations. In contrast to the lack of structural difference within the series **1a**, **2a**, **4a**, **5a**, the nitro-substituted system $\mathbf{5a}^n$ is thus showing the expected shift of redox potentials and absorption spectra due to a significant stabilization of the lowest unoccupied molecular orbital (LUMO).

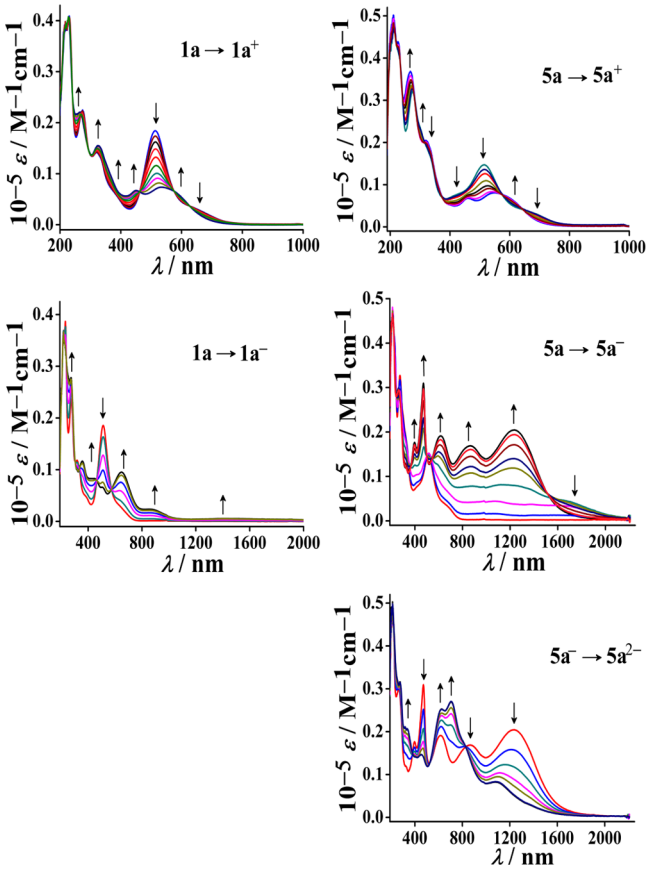

Figure 5. UV−vis−NIR spectroelectrochemistry of $\mathbf{1a}^n$ (left) and $\mathbf{5a}^n$ (right) in CH_3CN/0.1 M NBu_4PF_6.

dx.doi.org/10.1021/ic500730m | Inorg. Chem. 2014, 53, 7389−7403

Table 6. UV−vis−NIR Spectroelectrochemical Data of 1a^n, 2a^n, 4a^n, and 5a^n in CH_3CN/0.1 M Bu_4NPF_6

complex	λ [nm] (ε [M^{-1} cm^{-1}])
1a$^+$	546(7250), 452(6670), 325(15460)
1a	650(sh), 516(18330), 322(13260)
1a$^-$	1417(560), 891(2230), 647(9520), 451(8260), 355(11650)
2a$^+$	535(5900), 449(6390), 329(11140)
2a	646(sh), 516(14450), 331(10430)
2a$^-$	1432(500), 874(1830), 653(8270), 445(6700), 361(9360)
4a$^+$	545(6350), 451(6130), 326(12850)
4a	660(sh), 512(15660), 324(13100)
4a$^-$	1408(600), 909(2400), 641(8850), 439(8010), 361(11080)
5a$^+$	562(7940), 459(6780), 322(20240)
5a	671(sh), 514(14690), 334(sh)
5a$^-$	1236(20450), 867(16900), 618(19110), 469(30760), 397(17660)
5a^{2-}	1100(8260), 712(26930), 624(25200), 457(14620), 338(20590)

Structural Investigation of {(μ-tppz)[RuCl(BIAN)$_2$]$_2$}-(ClO$_4$)$_2$. The identity of the tppz-bridged diruthenium complexes [**1b**](ClO$_4$)$_2$−[**4b**](ClO$_4$)$_2$ was established via single-crystal X-ray structure determination of the representative compounds [**2b**](ClO$_4$)$_2$ and [**3b**](ClO$_4$)$_2$ (Figures 6 and 7, Tables 1 and 8, and Tables S17−S19 of the Supporting Information). The crystal structures exhibit *trans* configurations with respect to the mutual orientation of the chloride ligands. The distorted octahedral arrangement around the ruthenium centers is reflected by the smaller chelate bite angles (<90°) as well as by the diminished *trans* angles (<180°) (Table S18, Supporting Information). Specifically, the steric constraints due to the meridionally coordinated nonplanar bis-tridentate tppz ligand[13,27] result in intraligand *trans* angles of about 160°. The nonplanarity of the bridging tppz ligand leads to pyridine/pyridine dihedral angles of about 40−50°; the dihedral angles between the central pyrazine ring and the pyridine rings of tppz lie between 19° and 27°. The slightly nonplanar pyrazine rings in [**2b**](ClO$_4$)$_2$ and [**3b**](ClO$_4$)$_2$ exhibit folding angles[13,28] of about 3.4°.

The average Ru−N(pyrazine, tppz) distances of 1.948 and 1.947 Å in [**2b**](ClO$_4$)$_2$ and [**3b**](ClO$_4$)$_2$ are appreciably shorter than the corresponding average Ru−N(pyridine, tppz) distances of 2.057 and 2.065 Å, respectively. The associated stronger (dπ)Ru → (pπ*) pyrazine(tppz) back-bonding facilitates the tppz-mediated intermetallic electronic coupling in the mixed-valent {Ru^{III}(μ-tppz)Ru^{II}} state (see later).[13] In both [**2b**](ClO$_4$)$_2$ and [**3b**](ClO$_4$)$_2$, the Ru−N(BIAN) distances *trans* to the Ru−N(pyrazine, tppz) bonds are considerably longer (by 0.049−0.086 Å) than the corresponding Ru−N(BIAN) distances *trans* to Ru−Cl, reflecting the stronger Ru → N(pyrazine, tppz) back-bonding. Although the low crystal quality of [**2b**](ClO$_4$)$_2$·H$_2$O results in diminished significance of the metric parameters, the intrachelate N−C and C−C distances of the coordinated BIAN ligands in the dinuclear complexes [**2b**](ClO$_4$)$_2$ and [**3b**](ClO$_4$)$_2$ are distinct from those in the mononuclear complexes **1a**, **2a**, **4a**, and **5a** (Tables 2 and 8). The shorter N−C bonds (<1.31 Å) and longer intrachelate C−C distance (1.478 Å) in the tppz complexes reflects the competition between the π acceptors tppz and BIAN for the charge from the π-donating ruthenium(II). As a consequence, the BIAN ligand is considered to remain unreduced in the complex series **1b**$^{2+}$−**4b**$^{2+}$.

The Cl···Cl/Ru···Ru separations in [**2b**](ClO$_4$)$_2$ and [**3b**](ClO$_4$)$_2$ are 8.114/6.558 Å and 8.331/6.558 Å, respectively. The DFT-optimized structure of **2b**$^{2+}$ (Figure S15 and Tables S17−S19, Supporting Information) reproduces the experimental structure rather well.

Electrochemistry and Spectroelectrochemistry of {(μ-tppz)[Ru(Cl)(BIAN)]$_2$}(ClO$_4$)$_2$. The tppz-bridged diruthenium complexes [**1b**](ClO$_4$)$_2$−[**4b**](ClO$_4$)$_2$ exhibit two reversible oxidation processes, corresponding to Ru^{II}Ru^{II} ⇌ Ru^{III}Ru^{II} (Ox1) and Ru^{III}Ru^{II} ⇌ Ru^{III}Ru^{III} (Ox2), with typical K_c values of 10^4 (RT ln(K_c) = $nF(\Delta E)$; Figure 8, Table 9). The

Table 7a. TD-DFT (B3LYP/CPCM/CH_3CN) Calculated Electronic Transitions for 1a^n

λ [nm] expt. (DFT)	ε [M^{-1} cm^{-1}] (f)	transitions	character
		1a (S = 0)	
650 (593)	sh (0.044)	HOMO−1→LUMO(0.54)	Ru(dπ)→BIAN(π*)
		HOMO→LUMO+1(0.43	Ru(dπ)→BIAN(π*)
516 (503)	18330 (0.200)	HOMO→LUMO+1(0.51)	Ru(dπ)→BIAN(π*)
		HOMO−2→LUMO+1(0.28)	Ru(dπ)→BIAN(π*)
322 (330)	13260 (0.050)	HOMO−8→LUMO(0.52)	BIAN(π)→BIAN(π*)
		HOMO−11→LUMO(0.33)	BIAN(π)→BIAN(π*)
		1a$^+$ (S = 1/2)	
546 (558)	7250 (0.044)	HOMO−4(β)→LUMO(β)(0.73)	BIAN(π)→Ru(dπ)
		HOMO−3(β)→LUMO(β)(0.40)	acac(π)/Ru(dπ)→Ru(dπ)
452 (452)	6670 (0.091)	SOMO-2(α)→LUMO(α)(0.58)	BIAN(π)→BIAN(π*)
		HOMO−1(β)→LUMO+1(β)(0.49)	BIAN(π)/ acac(π)→BIAN(π*)
325 (357)	15460 (0.142)	HOMO(β)→LUMO+2(β)(0.78)	acac(π)→BIAN(π*)
		SOMO-1(α)→LUMO+1(α)(0.53)	acac(π)→BIAN(π*)
		1a$^-$ (S = 1/2)	
1417 (1429)	560 (0.018)	SOMO(α)→LUMO(α)(0.99)	BIAN(π)→BIAN(π*)
891 (771)	2230 (0.057)	HOMO−1(β)→LUMO(β)(0.90)	Ru(dπ)→BIAN(π*)
647 (568)	9520 (0.144)	SOMO-1(α)→LUMO(α)(0.65)	Ru(dπ)→BIAN(π*)
		HOMO(β)→LUMO+1(β)(0.56)	Ru(dπ)→BIAN(π*)
451 (430)	8260 (0.076)	HOMO−3(β)→LUMO(β)(0.73)	BIAN(π)→BIAN(π*)
355 (355)	11650 (0.077)	HOMO−4(β)→LUMO(β)(0.47)	acac(π)→BIAN(π*)
		HOMO−6(β)→LUMO(β)(0.39)	BIAN(π)→BIAN(π*)

dx.doi.org/10.1021/ic500730m | Inorg. Chem. 2014, 53, 7389−7403

Table 7b. TD-DFT (B3LYP/CPCM/CH_3CN) Calculated Electronic Transitions for 5a[n]

λ [nm] expt. (DFT)	ε [M^{-1} cm^{-1}] (f)	transitions	character
		5a (S = 0)	
671 (659)	sh (0.022)	HOMO→LUMO+1(0.53)	Ru(dπ)→BIAN(π^*)
514 (501)	14690 (0.051)	HOMO−2→LUMO+2(0.64)	Ru(dπ)→BIAN(π^*)
334 (346)	sh (0.145)	HOMO−8→LUMO(0.50)	BIAN(π)→BIAN(π^*)
		5a$^+$ (S = 1/2)	
562 (585)	7940 (0.059)	HOMO−1(β)→LUMO(β)(0.65)	acac(π)/BIAN(π)→Ru(dπ)
459 (473)	6780 (0.099)	SOMO-2(α)→LUMO(α)(0.61)	BIAN(π)→BIAN(π^*)
		HOMO(β)→LUMO+1(β)(0.54)	acac(π)→BIAN(π^*)
322 (321)	20240 (0.034)	SOMO-10(α)→LUMO(α)(0.48)	BIAN(π)→BIAN(π^*)
		HOMO−10(β)→LUMO+1(β)(0.42)	BIAN(π)→BIAN(π^*)
		5a$^-$ (S = 1/2)	
1236 (1066)	20450 (0.037)	HOMO−1(β)→LUMO(β)(0.53)	Ru(dπ)→BIAN(π^*)
867 (737)	16900 (0.015)	HOMO(β)→LUMO+1(β)(0.92)	Ru(dπ)→BIAN(π^*)
618 (691)	19110 (0.032)	HOMO−1(β)→LUMO+1(β)(0.84)	Ru(dπ)→BIAN(π^*)
469 (496)	30760 (0.139)	HOMO−3(β)→LUMO(β)(0.90)	acac(π)→BIAN(π^*)
397 (399)	17660 (0.095)	SOMO-4(α)→LUMO(α)(0.67)	acac(π)→BIAN(π^*)
		HOMO−3(β)→LUMO+1(β)(0.63)	acac(π)→BIAN(π^*)
		5a^{2-} (S = 0)	
1100 (908)	8260 (0.011)	HOMO−1→LUMO(0.70)	Ru(dπ)→BIAN(π^*)
712 (657)	26930 (0.302)	HOMO−3→LUMO(0.59)	Ru(dπ)→BIAN(π^*)
624 (574)	25200 (0.135)	HOMO−2→LUMO+1(0.66)	Ru(dπ)→BIAN(π^*)
457 (497)	14620 (0.140)	HOMO−2→LUMO+2(0.46)	Ru(dπ)→BIAN(π^*)
338 (348)	20590 (0.272)	HOMO−7→LUMO(0.63)	BIAN(π)→BIAN(π^*)

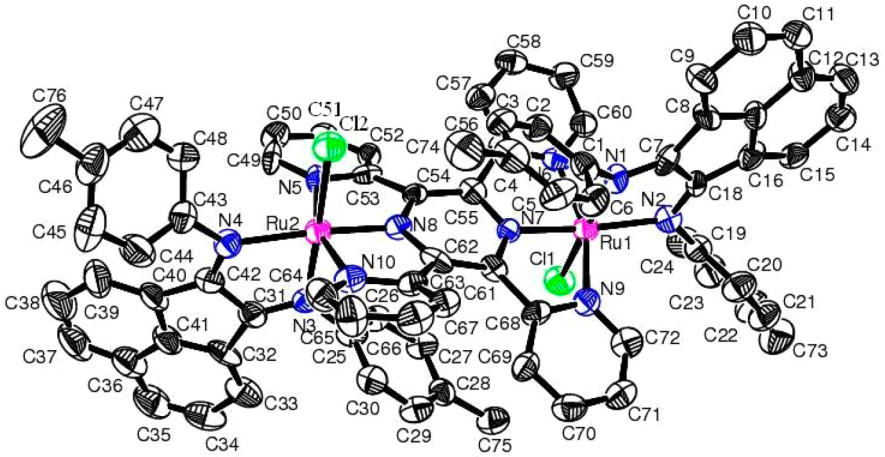

Figure 6. ORTEP diagram of [**2b**]$(ClO_4)_2$. Ellipsoids are drawn at the 50% probability level. Hydrogen atoms and solvent molecules are omitted for clarity.

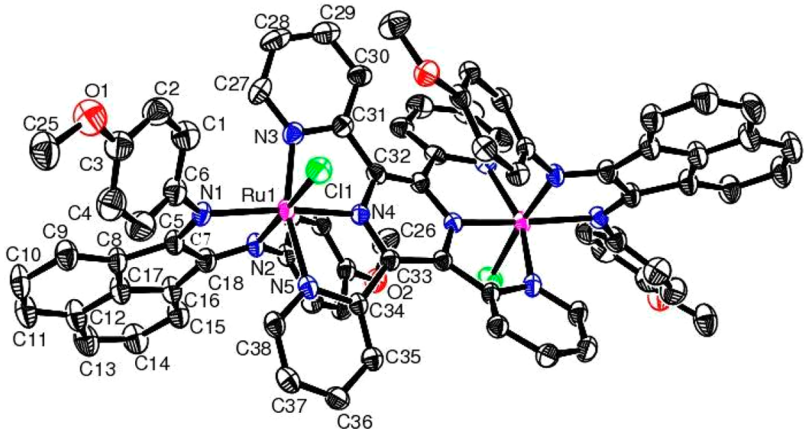

Figure 7. ORTEP diagram of [**3b**]$(ClO_4)_2$. Ellipsoids are drawn at the 50% probability level. Hydrogen atoms are omitted for clarity.

dx.doi.org/10.1021/ic500730m | Inorg. Chem. 2014, 53, 7389−7403

Table 8. Selected Experimental Bond Lengths (Å) for $[2b](ClO_4)_2 \cdot 0.5\ H_2O$ and $[3b](ClO_4)_2$

bond length (Å)	$[2b](ClO_4)_2 \cdot 0.5\ H_2O$	$[3b](ClO_4)_2$
Ru(1)−N(1)	2.032(9)	2.107(3)
Ru(1)−N(2)	2.056(9)	2.020(3)
Ru(1)−N(3)		2.072(3)
Ru(1)−N(4)		1.947(3)
Ru(1)−N(5)		2.059(3)
Ru(1)−N(6)	2.053(10)	
Ru(1)−N(7)	1.947(9)	
Ru(1)−N(9)	2.053(11)	
Ru(1)−Cl(1)	2.370(3)	2.3784(10)
N(1)−C(7)	1.271(15)	1.303(5)
N(2)−C(18)	1.291(14)	1.299(5)
C(7)−C(18)	1.478(16)	1.478(5)
Ru(2)−N(3)	2.027(9)	
Ru(2)−N(4)	2.101(9)	
Ru(2)−N(5)	2.062(10)	
Ru(2)−N(8)	1.949(8)	
Ru(2)−N(10)	2.058(11)	
Ru(2)−Cl(2)	2.387(3)	
N(3)−C(31)	1.319(15)	
N(4)−C(42)	1.298(15)	
C(31)−C(42)	1.453(18)	

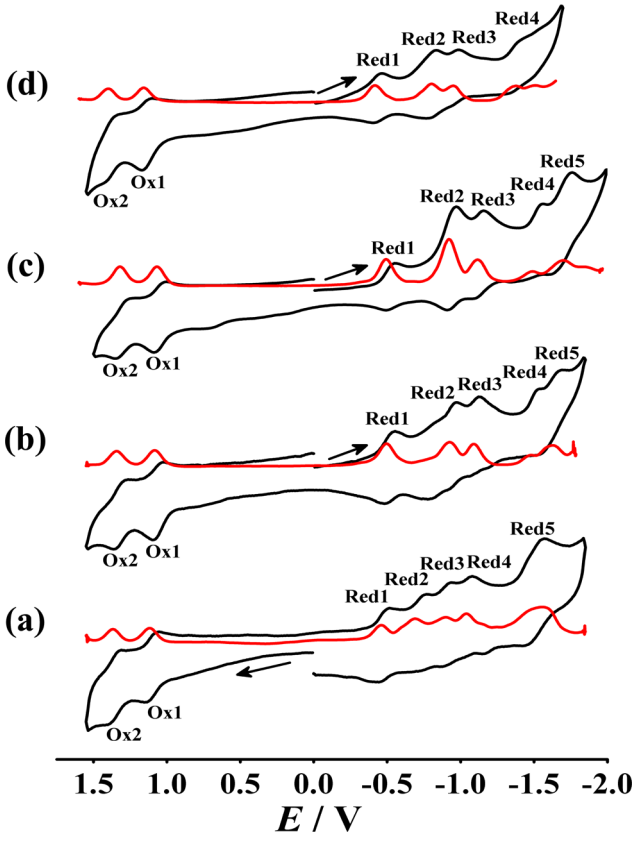

Figure 8. Cyclic voltammograms (black) and differential pulse voltammograms (red) of (a) $[1b](ClO_4)_2$, (b) $[2b](ClO_4)_2$, (c) $[3b](ClO_4)_2$, and (d) $[4b](ClO_4)_2$ in CH_3CN/0.1 M NEt_4ClO_4 at 298 K. Scan rate: 100 mV s^{-1}.

complexes also display multiple close-lying (tppz and BIAN) ligand-based reduction processes. Pyrazine and its substituted

Table 9. Electrochemical Data[a] for $[1b](ClO_4)_2$−$[4b](ClO_4)_2$

	$E^{\circ}_{298}[V](\Delta E[mV])^b$							$K_c{}^c$					
complex	Ox2	Ox1	Red1	Red2	Red3	Red4	Red5	$K_{c1}{}^d$	$K_{c2}{}^d$	$K_{c3}{}^d$	$K_{c4}{}^d$	$K_{c5}{}^d$	$K_{c6}{}^d$
$[1b](ClO_4)_2$	1.36 (80)	1.11 (80)	−0.46 (80)	−0.70 (100)	−0.90 (50)	−1.12 (80)	−1.51 (110)	2×10^4	4×10^{26}	2×10^4	2×10^3	5×10^3	4×10^6
$[2b](ClO_4)_2$	1.32 (80)	1.06 (60)	−0.52 (80)	−0.88 (180)	−1.10 (60)	−1.52 (ir)	−1.61 (140)	3×10^4	6×10^{26}	1×10^6	5×10^3	1×10^7	3×10^1
$[3b](ClO_4)_2$	1.29 (80)	1.04 (80)	−0.52 (60)	−0.93 (60)	−1.13 (60)	−1.48 (140)	−1.69 (140)	2×10^4	3×10^{26}	9×10^6	2×10^3	9×10^5	4×10^3
$[4b](ClO_4)_2$	1.38 (80)	1.14 (60)	−0.43 (60)	0.80 (60)	−0.97 (40)	−1.36 (80)		1×10^4	4×10^{26}	2×10^6	7×10^2	4×10^6	

[a]From cyclic voltammetry in CH_3CN/0.1 M Et_4NClO_4 at 100 mV s^{-1}. [b]Potential in V versus SCE; peak potential differences ΔE_p/mV (in parentheses). [c]Comproportionation constant from $RT \ln K_c = nF(\Delta E)$. [d]$K_{c1}$ between Ox1 and Ox2; K_{c2} between Ox1 and Red1; K_{c3} between Red1 and Red2; K_{c4} between Red2 and Red3; K_{c5} between Red3 and Red4; K_{c6} between Red4 and Red5.

dx.doi.org/10.1021/ic500730m | Inorg. Chem. 2014, 53, 7389−7403

derivatives like tppz have a pronounced tendency for facile stepwise reduction by two electrons.[13,28]

Slight variations of the redox potentials occur depending on the electron-donating and -withdrawing substituents at BIAN in $[\mathbf{1b}](ClO_4)_2$–$[\mathbf{4b}](ClO_4)_2$.

The rather low K_c values of about 10^4 for the mixed-valent trications reflect the relatively strong π electron-acceptor effect of BIAN: π acceptors as ancillary ligands tend to diminish the metal–metal interaction in acceptor-bridged dinuclear systems due to competition with the bridge, confirming an "electron transfer" mechanism of valence exchange.[13b,27,29] Comparable values were observed with 2-phenylazopyridine (pap) as ancillary ligands,[30] whereas $acac^-$ and related donor coligands cause the opposite effect with strong metal–metal interaction ($K_c = 10^{12}$).[31]

The oxidatively electrogenerated trications do not exhibit any EPR signals even at 4 K. Such a behavior is well-known for weakly coupled $Ru^{III}Ru^{II}$ mixed-valent compounds;[27,29] the EPR "silence" is caused by the rapid relaxation due to close-lying excited states and the high spin–orbit coupling contributions from the metals.[27]

The reductively electrogenerated monocations display unresolved EPR signals at about $g = 2.0$ (Figure S19, Supporting Information) which signify radical complexes[26] and thus support the notion of $tppz^{\bullet-}$ formation.[13,30,31] The first reduction potentials of the free ligands tppz and BIAN lie at −0.94 V and −1.40 V, respectively, versus SCE in acetonitrile, confirming that tppz is the better π acceptor.

The calculated spin density (Table 10) for the representative case $\mathbf{2b}^+$ with largely tppz-centered spin is confirmed by the EPR g factors close to the free-electron value of 2.0023 (Figure S19, Supporting Information). The calculated metal-based spin for $\mathbf{2b}^{3+}$ is in agreement with the experiment, that is, EPR silence even at 4 K, especially considering the DFT-suggested localization of the valences (Figure 9; Class II according to Robin and Day[32]). The further oxidized species $\mathbf{2b}^{4+}$ is calculated with a triplet ground state reflecting the diruthenium(III) situation, while the highly reduced $\mathbf{2b}^-$ is calculated as an $S = 1/2$ species with two coupled BIAN radical anion ligands and a $tppz^{\bullet-}$ bridge (Tables S16 and S20–26, Supporting Information).

Table 10. DFT-Calculated Mulliken Spin Distributions for 2b″

complex	Ru	tppz	BIAN	Cl
$\mathbf{2b}^{4+}$ ($S = 1$)	1.194	0.001	0.482	0.239
$\mathbf{2b}^{3+}$ ($S = 1/2$)	0.759	0.001	0.085	0.152
$\mathbf{2b}^{+}$ ($S = 1/2$)	−0.005	0.964	0.047	−0.002
$\mathbf{2b}^{-}$ ($S = 1/2$)	0.160	−0.938	1.766	0

TD-DFT calculations (Table 12) confirmed the observed absorptions and were used for the assignment of transitions. The most conspicuous change on oxidation, for example, of $\mathbf{2b}^{2+}$ to Ru^{II}/Ru^{III} mixed-valent $\mathbf{2b}^{3+}$, is the appearance of the intervalence charge transfer (IVCT) band at about 1820 nm, that is, in the expected[33] NIR region (Figure 10, Table 11, and Figures S16–S18 and Table S27 of the Supporting Information). Confirming the Class II assignment,[32] this band is rather weak and broad (Table 11). The MLCT absorption of $\mathbf{2b}^{2+}$ at about 600 nm remains little changed. The second oxidation to homovalent (Ru^{III}/Ru^{III}) $\mathbf{2b}^{4+}$ causes the IVCT band to disappear, and a new long-wavelength absorption at 966 nm is attributed to an LMCT process.

On reduction of $\mathbf{2b}^{2+}$ to $\mathbf{2b}^+$ the characteristic[13,31] intraligand (IL) transition of $tppz^{\bullet-}$ appears as a small narrow band at 1046 nm, followed by a ligand-to-ligand (interligand) charge transfer (LLCT) at $\lambda_{max} = 915$ nm. The MLCT absorption remains at about 620 nm. Further reduction to $\mathbf{2b}^0$ produces long-wavelength bands at 1135 and 637 nm, resulting from transitions based on the HOMO of $tppz^{2-}$. The following electron uptake to $\mathbf{2b}^-$ shows similar absorptions, and the final member, $\mathbf{2b}^{2-}$, in that series has NIR absorptions that are involving the various reduced ligands (Table 12).

CONCLUSION

The BIAN ligands are strongly π-accepting α-diimines, comparable in their redox potentials to 1,4-diaryl-1,4-diazabuta-1,3-dienes[17] or 2-phenylazopyridine (pap).[30] In addition to their preformed *s-cis* chelate structures, a remarkable special feature of the BIAN ligands with their distortion due to the C_5 ring is the enhanced sensitivity of the C–C bond connected by the peri C atoms in the 1,8-positions of the naphthalene core. The strain as reflected by the 105°/135° angles (Chart 1) leads to a rather significant shortening of that diagnostic[6] C–C bond from long values of >1.52 Å for the free ligands via about 1.49 Å in "normal" complexes with little π-donating metals to 1.44 Å for the ruthenium compounds $[Ru(acac)_2(BIAN)]$ as described here. The 1.44 Å bond length agrees with the value reported for the Na^+ salt of a BIAN anion radical,[4a] while the second reduction to a dianion causes a further decrease of d(CC) to about 1.40 Å.[4] In contrast, the tppz-bridged dinuclear systems $\{(\mu\text{-tppz})[Ru(Cl)(BIAN)]_2\}(ClO_4)_2$ contain unreduced BIAN ligands because of the competion from tppz for the metal donor π charge.

According to the structure data alone, a $Ru^{III}(BIAN^{\bullet-})$ oxidation state formulation would therefore be justified.[17] However, in conjunction with DFT calculations results the EPR data revealing Ru^{III}-containing cations and $BIAN^{\bullet-}$-containing anions rather suggest an ambiguous resonance situation $Ru^{III}(BIAN^{\bullet-})/Ru^{II}(BIAN^0)$ (see Scheme 3), with considerable charge transfer in the ground state.

A noted consequence of the significant π-acceptor character of the BIAN terminal ligands in dinuclear compounds $\{(\mu\text{-tppz})[Ru(Cl)(BIAN)]_2\}^n$, tppz = 2,3,5,6-tetrakis(2-pyridyl)-pyrazine, is to decrease the metal–metal interaction of the $Ru^{III}Ru^{II}$ mixed-valent state ($n = 3+$) due to competition with the similarly π-accepting bridge tppz for the π-electron density of the metals. The small K_c values, the low intensity of the corresponding intervalence charge transfer (IVCT) transition in the NIR, and the absence of an EPR signal even at 4 K confirm a weak metal–metal interaction.

In contrast to what may be expected from an unreflected MO analysis there was no evidence in our experiments for the acquisition by BIAN of more than two electrons.[2,4] Such excess reduction will require the presence of charge-compensating cations,[4] but neither $[Ru(acac)_2(BIAN)]^n$ (with $acac^-$ donors) nor $\{(\mu\text{-tppz})[Ru(Cl)(BIAN)]_2\}^n$ systems (with the competing tppz acceptor) meet this requirement. Nonetheless, the BIAN ligands have a potential for multiple site-separated reduction, while their strained carbon framework offers a sensitive diagnostic parameter for assessing the metal-to-ligand π charge donation in corresponding chelate compounds.

dx.doi.org/10.1021/ic500730m | Inorg. Chem. 2014, 53, 7389–7403

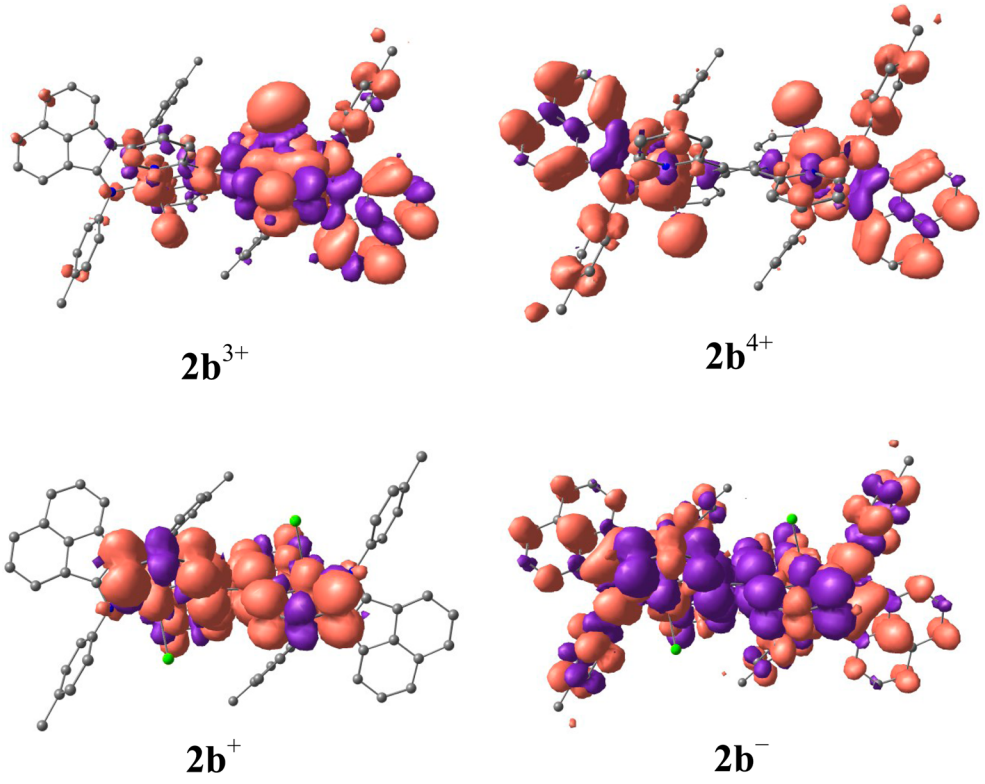

Figure 9. DFT-calculated Mulliken spin-density plots of **2b**^{n}.

Table 11. UV−vis−NIR Spectroelectrochemical Data of 2b^{n} in CH_3CN/0.1 M Bu_4NPF_6

complex	λ [nm] (ε [M^{-1} cm^{-1}])
2b^{4+}	966(3120), 540(sh), 399(43730), 314(36190)
2b^{3+}	1831(1900), 608(19510), 384(40440), 328(sh), 312(35150)
2b^{2+}	622(37710), 433(sh), 381(37000), 366(36980), 331(31220), 302(36400)
2b^{+}	1046(9330), 915(4900), 618(40400), 442(29020), 403(31580), 369(29250), 312(37200)
2b	1143(sh), 978(6630), 637(25690), 483(sh), 438(31360), 397(32980), 368(33720), 305(39780)
2b^{-}	1183(sh), 676(22310), 438(32680), 369(37800), 307(42450)
2b^{2-}	1041(1210), 918(8180), 662(23420), 428(35840), 356(40870), 310(sh)

EXPERIMENTAL SECTION

Materials. The metal precursors $[Ru^{II}(acac)_2(CH_3CN)_2]$,[34] $[Cl_3Ru^{III}(\mu\text{-tppz})Ru^{III}Cl_3]$[35] and the ligands (*N*,*N*′-diarylacenaphthoquinonediimines)[36] were prepared according to the literature procedures. All other chemicals and reagents were of reagent grade and were used without further purification. For spectroscopic and electrochemical studies high-performance liquid chromatography (HPLC) grade solvents were used.

Physical Measurements. UV−vis−NIR spectroelectrochemical studies were performed in CH_3CN/0.1 M Bu_4NPF_6 at 298 K, using an optically transparent thin layer electrochemical (OTTLE) cell,[37] which was mounted in the sample compartment of a J&M TIDAS spectrophotometer. Fourier transform infrared (FT-IR) spectra were taken on a Nicolet spectrophotometer with samples prepared as KBr pellets. ^{1}H NMR spectra were recorded on a Bruker Avance III 400 spectrometer. The EPR measurements were made in a two-electrode capillary tube[26b] with an X-band Bruker system ESP300 equipped with a Bruker ER035 M gaussmeter and a HP 5350B microwave counter. Cyclic voltammetric, differential pulse voltammetric, and coulometric measurements were carried out using a PAR model 273A electrochemistry system. Platinum wire working and auxiliary electrodes and an aqueous saturated calomel reference electrode (SCE) were used in a three-electrode configuration. The supporting electrolyte was $[Et_4N][ClO_4]$, and the solute concentration was ~10^{-3} M. The half-wave potential E°_{298} was set equal to 0.5(E_{pa} + E_{pc}), where E_{pa} and E_{pc} are anodic and cathodic cyclic voltammetric peak potentials, respectively. The electrical conductivities of the complexes in CH_3CN were checked with an Autoranging conductivity meter (Toshcon Industries, India). The elemental analysis was carried out on a Thermoquest (EA 1112) microanalyzer. Electrospray ionization mass spectra (ESI-MS) were recorded on a Micromass Q-ToF mass spectrometer.

Crystallography. Single crystals of **1a**, **2a**, **4a**, and **5a** were grown by slow evaporation of their 2:1 dichloromethane−*n*-hexane solutions, while those of $[\mathbf{2b}](ClO_4)_2$ and $[\mathbf{3b}](ClO_4)_2$ were obtained by gradual evaporation of their 1:1 dichloromethane−methanol solutions. X-ray crystal data were collected on a CCD Agilent Technologies (Oxford Diffraction) SUPER NOVA diffractometer. Data collection was evaluated by using the CrysAlisPro CCD software. The data were collected by the standard $\varphi-\omega$ scan techniques and were scaled and reduced using CrysAlisPro RED software. The structures were solved by direct method using SHELXS-97 and refined by full matrix least-squares with SHELXL-97, refining on F^2.[38] All non-hydrogen atoms were refined anisotropically. The remaining hydrogen atoms were placed in geometrically constrained positions and were refined with isotropic temperature factors, generally 1.2U_{eq} of their parent atoms. Hydrogen atoms were included in the refinement process as per the riding model. The hydrogen atom of the water molecule in $[\mathbf{2b}](ClO_4)_2\cdot 0.5H_2O$ could not be located, but its contribution was considered in calculating the molecular composition in Table 1.

Computational Details. Full geometry optimizations were carried out by using the DFT method at the (R)B3LYP level for **1a**, **5a**, **5a**$^{2-}$, **2b**$^{2+}$, **2b**, and **2b**$^{2-}$ and at the (U)B3LYP level for **1a**$^{+}$, **5a**$^{+}$, **1a**$^{-}$, **5a**$^{-}$, **2b**$^{3+}$, **2b**$^{4+}$, **2b**$^{+}$, and **2b**$^{-}$.[39] Except for ruthenium, all elements were assigned the 6-31G* basis set. The LANL2DZ basis set with effective core potential was employed for the ruthenium atom.[40] The vibrational frequency calculations were performed to ensure that the optimized geometries represent the local minima, and there are only positive eigenvalues. All calculations were performed with the

dx.doi.org/10.1021/ic500730m | Inorg. Chem. 2014, 53, 7389−7403

Table 12. TD-DFT (B3LYP/CPCM/CH_3CN) Calculated Electronic Transitions for 2b^n

λ [nm] expt (DFT)	ε [M^{-1} cm^{-1}] (f)	transitions	character
		2b^{2+} (S = 0)	
622 (626)	37710 (0.03)	HOMO→LUMO+3(0.39)	Ru(dπ)→BIAN(π^*)
		HOMO−1→LUMO+1(0.37)	Ru(dπ)→tppz(π^*)
		HOMO−1→LUMO+2(0.36)	Ru(dπ)→BIAN(π^*)
433 (441)	sh (0.03)	HOMO−4→LUMO+3(0.45)	BIAN(π)→BIAN(π^*)
381 (393)	37000 (0.09)	HOMO+12→LUMO(0.41)	BIAN(π)→tppz(π^*)
366 (373)	36980 (0.09)	HOMO−12→LUMO+1(0.35)	BIAN(π)→tppz(π^*)
331 (340)	31220 (0.03)	HOMO−7→LUMO+5(0.37)	BIAN(π)→BIAN(π^*)
302 (310)	36400 (0.06)	HOMO−10→LUMO+5(0.40)	BIAN(π)→BIAN(π^*)
		2b^{3+} (S = 1/2)	
1831 (1874)	1900 (0.008)	HOMO(β)→LUMO(β)(0.95)	Ru(dπ)→Ru(dπ)
608 (601)	19510 (0.05)	HOMO(β)→LUMO+4(β)(0.56)	Ru(dπ)→BIAN(π^*)
384 (397)	40440 (0.12)	HOMO−11(β)→LUMO+3(β)(0.51)	Ru(dπ)→BIAN(π^*)
331 (337)	sh (0.02)	SOMO-5(α)→LUMO+5(α)(0.33)	BIAN(π)/Cl(π)→BIAN(π^*)
		2b^{4+} (S = 1)	
966 (1007)	3120 (0.02)	HOMO−1(β)→LUMO+1(β)(0.53)	BIAN(π)→Ru(dπ)
540 (530)	sh (0.03)	HOMO(β)→LUMO+4(β)(0.41)	BIAN(π)→BIAN(π^*)
399 (405)	43730 (0.13)	SOMO1−12(α)→LUMO(α)(0.55)	BIAN(π)→tppz(π^*)
314 (340)	36190 (0.02)	SOMO1(α)→LUMO+9(α)(0.30)	BIAN(π)→tppz(π^*)
		2b^{+} (S = 1/2)	
1046 (973)	9330 (0.09)	SOMO(α)→LUMO+5(α)(0.96)	tppz(π)→tppz(π^*)
915 (889)	4900 (0.002)	SOMO(α)→LUMO+3(α)(0.75)	tppz(π)→BIAN(π^*)
618 (645)	40400 (0.05)	SOMO-2(α)→LUMO+2(α)(0.57)	Ru(dπ)→tppz(π^*)
442 (445)	29020 (0.12)	SOMO(α)→LUMO+12(α)(0.51)	tppz(π)→tppz(π^*)
		SOMO(α)→LUMO+14(α)(0.49)	tppz(π)→BIAN(π^*)/ Ru(dπ)
403 (400)	31580 (0.14)	HOMO−9(β)→LUMO+1(β)(0.35)	BIAN(π)→BIAN(π^*)
		SOMO-9(α)→LUMO+1(α)(0.31)	BIAN(π)→BIAN(π^*)
369 (378)	29250 (0.08)	SOMO-9(α)→LUMO+2(α)(0.59)	BIAN(π^*)→tppz(π)
312 (319)	37200 (0.04)	HOMO−14(β)→LUMO+1(β)(0.39)	BIAN(π)/Cl(π)→BIAN(π^*)
		2b (S = 0)	
1143 (1188)	sh (0.005)	HOMO→LUMO+3(0.70)	tppz(π)→BIAN(π^*)
978 (886)	6630 (0.14)	HOMO→LUMO+5(0.70)	tppz(π)→tppz(π^*)
637 (589)	25690 (0.06)	HOMO→LUMO+8(0.66)	tppz(π)→BIAN(π^*)
637 (572)	25690 (0.10)	HOMO→LUMO+7(0.64)	tppz(π)→tppz(π^*)
483 (487)	sh (0.08)	HOMO−3→LUMO+2(0.41)	Ru(dπ)→BIAN(π^*)
438 (443)	31360 (0.12)	HOMO+8→LUMO(0.45)	BIAN(π)→BIAN(π^*)
		HOMO+7→LUMO+1(0.37)	tppz(π)→BIAN(π^*)
397 (393)	32980 (0.13)	HOMO−10→LUMO(0.53)	Cl(π)/BIAN(π)→BIAN(π^*)
368 (383)	33720 (0.28)	HOMO−12→LUMO+2(0.59)	Cl(π)/BIAN(π)→BIAN(π^*)
305 (294)	39780 (0.11)	HOMO−23→LUMO+1(0.34)	BIAN(π)→BIAN(π^*)
		2b^{-} (S = 1/2)	
1183 (1203)	sh (0.02)	HOMO(β)→LUMO+3(β)(0.71)	tppz(π)→BIAN(π^*)
		SOMO(α)→LUMO+2(α)(0.70)	BIAN(π)→BIAN(π^*)
676 (637)	22310 (0.0.6)	SOMO(α)→LUMO+6(α)(0.42)	BIAN(π)→tppz(π^*)
676 (600)	22310 (0.17)	HOMO(β)→LUMO+6(β)(0.41)	tppz(π)→tppz(π^*)
		HOMO−2(β)→LUMO+2(β)(0.53)	Ru(dπ)→BIAN(π^*)
438 (434)	32680 (0.04)	HOMO−4(β)→LUMO+2(β)(0.73)	Ru(dπ)→BIAN(π^*)
369 (373)	37800 (0.10)	SOMO-10(α)→LUMO+1(α)(0.44)	BIAN(π)→tppz(π^*)
		HOMO−9(β)→LUMO+1(β)(0.43)	tppz(π)→tppz(π^*)
		2b^{2-} (S = 0)	
1041 (1247)	1210 (0.05)	HOMO→LUMO+4(0.67)	BIAN(π)→tppz(π^*)
1041 (1227)	1210 (0.05)	HOMO→LUMO+3(0.63)	BIAN(π)→BIAN(π^*)
918 (949)	8180 (0.10)	HOMO−1→LUMO+4(0.69)	tppz(π)→tppz(π^*)
662 (645)	23420 (0.10)	HOMO−5→LUMO(0.55)	Ru(dπ)→BIAN(π^*)
428 (433)	35840 (0.17)	HOMO−9→LUMO+1(0.45)	BIAN(π)→tppz(π^*)
428 (425)	35840 (0.15)	HOMO−10→LUMO(0.57)	tppz(π)→BIAN(π^*)
356 (367)	40870 (0.20)	HOMO→LUMO+23(0.61)	BIAN(π)→tppz(π^*)
310 (325)	sh (0.02)	HOMO−12→LUMO+4(0.61)	BIAN(π)→tppz(π^*)

dx.doi.org/10.1021/ic500730m | Inorg. Chem. 2014, 53, 7389−7403

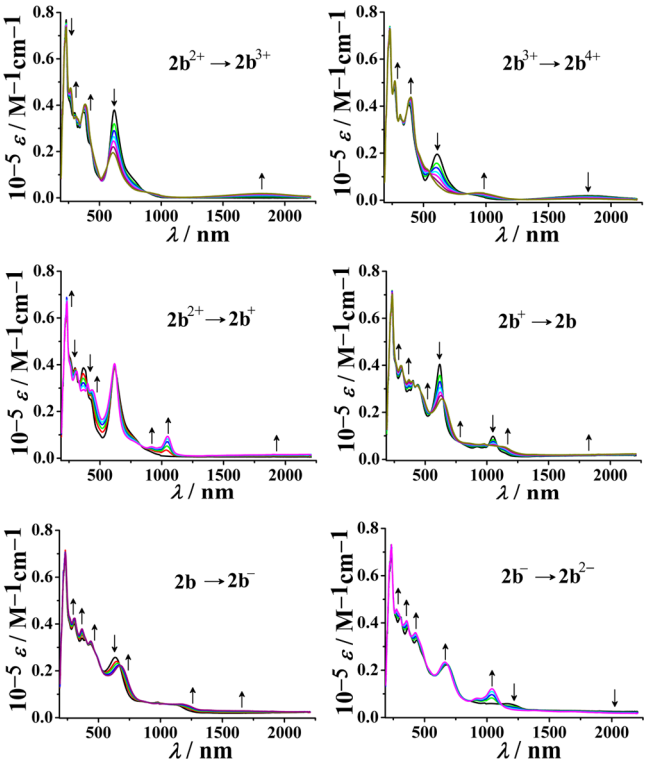

Figure 10. UV−vis−NIR spectroelectrochemistry of **2b**^{n} in CH_3CN/0.1 M NBu_4PF_6.

Scheme 4. Oxidation State Assignments for the [(BIAN)ClRu(μ-tppz)RuCl(BIAN)]^n Redox Series[a]

$$[(BIAN)ClRu^{III}(\mu\text{-tppz})Ru^{III}Cl(BIAN)]^{4+}$$
$$\overset{-e^-}{\underset{+e^-}{\rightleftharpoons}}$$
$$[(BIAN)ClRu^{III}(\mu\text{-tppz})Ru^{II}Cl(BIAN)]^{3+}$$
$$\overset{-e^-}{\underset{+e^-}{\rightleftharpoons}}$$
$$[(BIAN)ClRu^{II}(\mu\text{-tppz})Ru^{II}Cl(BIAN)]^{2+}$$
$$\overset{-e^-}{\underset{+e^-}{\rightleftharpoons}}$$
$$[(BIAN)ClRu^{II}(\mu\text{-tppz}^{\bullet-})Ru^{II}Cl(BIAN)]^{+}$$
$$\overset{-e^-}{\underset{+e^-}{\rightleftharpoons}}$$
$$[(BIAN)ClRu^{II}(\mu\text{-tppz}^{2-})Ru^{II}Cl(BIAN)]^{0}$$
$$\overset{-e^-}{\underset{+e^-}{\rightleftharpoons}}$$
$$[(BIAN^{\bullet-})ClRu^{II}(\mu\text{-tppz}^{\bullet-})Ru^{II}Cl(BIAN^{\bullet-})]^{-}$$
$$\overset{-e^-}{\underset{+e^-}{\rightleftharpoons}}$$
$$[(BIAN^{\bullet-})ClRu^{II}(\mu\text{-tppz}^{2-})Ru^{II}Cl(BIAN^{\bullet-})]^{2-}$$

[a]From data obtained for **2b**^{n}.

Gaussian09 program package.[41] Vertical electronic excitations based on (R)B3LYP/(U)B3LYP optimized geometries were computed for **1a**^{n} (n = +1, 0, −1), **5a**^{n} (n = +1, 0, −1, −2), and **2b**^{n} (n = +4, +3, +2, +1, 0, −1, −2) using the TD-DFT formalism[42] in acetonitrile using conductor-like polarizable continuum model (CPCM).[43] *Chemissian 1.7*[44] was used to calculate the fractional contributions of various groups to each MO. All calculated structures were visualized with *ChemCraft*.[45]

Preparation of Complexes. The complexes **1a**−**5a** were prepared by following a general procedure. The method for the representative **1a** is given below.

Preparation of [Ru(acac)$_2$(BIAN)] 1a. The precursor complex [Ru^{II}(acac)$_2$(CH_3CN)$_2$] (100 mg, 0.260 mmol) and the ligand BIAN (R = H = (bis(phenyl)acenaphthenequinonediimine) (86 mg, 0.260 mmol) were mixed in 30 mL of ethanol, and this mixture was heated to reflux for 5 h under dinitrogen atmosphere. The color of the initially orange solution gradually changed to deep violet. The reaction mixture was evaporated to dryness under reduced pressure and purified by column chromatography on silica gel (mesh 60−120) column. The deep violet mononuclear complex **1a** was eluted by a solvent mixture of CH_2Cl_2−CH_3CN (100:1). Evaporation of solvent under reduced pressure yielded pure **1a**.

1a: Yield, 135 mg (82%). ^{1}H NMR in $(CD_3)_2SO$ [δ/ppm (J/Hz)]: 8.00 (d, 8.28, 1H), 7.44 (m, 3H), 7.40 (d, 8.16, 1H), 7.27 (b, 2H), 7.09 (d, 7.16, 1H), 5.12 (s, 1H, CH(acac)), 1.90 (s, 3H, CH_3(acac)), 1.55 (s, 3H, CH_3(acac)). MS (ESI+, CH_3CN): m/z {[M−H]$^+$} calcd: 632.69; found: 632.17. Anal. Calcd for $C_{34}H_{30}N_2O_4Ru$: C, 64.65; H, 4.79; N, 4.43; found: C, 64.62; H, 4.85; N, 4.50%.

2a: Yield, 146 mg (85%). ^{1}H NMR in $(CD_3)_2SO$ [δ/ppm (J/Hz)]: 8.00 (d, 8.24, 1H), 7.42 (t, 7.44, 8.04, 1H), 7.24 (d, 7.80, 2H), 7.15 (d, 7.16, 3H), 5.13 (s, 1H, CH(acac)), 2.37 (s, 3H, BIAN), 1.88 (s, 3H, CH_3(acac)), 1.57 (s, 3H, CH_3(acac)). MS (ESI+, CH_3CN): m/z {[M−H]$^+$} calcd: 660.74; found: 660.94. Anal. Calcd for $C_{36}H_{34}N_2O_4Ru$: C, 65.54; H, 5.19; N, 4.25; found: C, 65.50; H, 5.20; N, 4.23%.

3a: Yield, 160 mg (88%). ^{1}H NMR in $(CD_3)_2SO$ [δ/ppm (J/Hz)]: 8.00 (d, 8.24, 1H), 7.43 (t, 8.12, 7.36, 1H), 7.21 (d, 7.16, 3H), 7.00 (d, 8.84, 2H), 5.14 (s, 1H, CH(acac)), 3.83 (s, 3H, BIAN), 1.87 (s, 3H, CH_3(acac)), 1.61 (s, 3H, CH_3(acac)). MS (ESI+, CH_3CN): m/z {[M−H]$^+$} calcd: 692.75, found: 692.92. Anal. Calcd for $C_{36}H_{34}N_2O_6Ru$: C, 62.51; H, 4.95; N, 4.05; found: C, 62.50; H, 4.92; N, 4.02%.

4a: Yield, 144 mg (79%). ^{1}H NMR in $(CD_3)_2SO$ [δ/ppm (J/Hz)]: 8.06 (d, 8.24, 1H), 7.51 (t, 6.10, 5.56, 2H), 7.46 (d, 8.12, 1H), 7.31 (b, 2H), 7.22 (d, 7.16, 1H), 5.16 (s, 1H, CH(acac)), 1.90 (s, 3H, CH_3(acac)), 1.62 (s, 3H, CH_3(acac)). MS (ESI+, CH_3CN): m/z {[M−H]$^+$} calcd: 701.58; found: 699.83. Anal. Calcd for $C_{34}H_{28}Cl_2N_2O_4Ru$: C, 58.29; H, 4.03; N, 4.00; found: C, 58.25; H, 4.00; N, 4.02%.

5a: Yield, 147 mg (78%). ^{1}H NMR in $(CD_3)_2SO$ [δ/ppm (J/Hz)]: 8.34 (d, 8.48, 2H), 8.12 (d, 8.24, 1H), 7.57 (d, 7.68, 2H), 7.47 (t, 7.44, 8.08, 1H), 7.29 (d, 7.20, 1H), 5.16 (s, 1H, CH(acac)), 1.95 (s, 3H, CH_3(acac)), 1.61 (s, 3H, CH_3(acac)). MS (ESI+, CH_3CN): m/z {[M−H]$^+$} calcd: 722.69; found: 722.82. Anal. Calcd for $C_{34}H_{28}N_4O_8Ru$: C, 56.59; H, 3.91; N, 7.76; found: C, 56.52; H, 3.88; N, 7.80%.

The complexes [**1b**]$(ClO_4)_2$−[**4b**]$(ClO_4)_2$ were prepared by following a common procedure. The details for the representative [**1b**]$(ClO_4)_2$ are given below.

Preparation of {(μ-tppz)[RuCl(BIAN)$_2$]$_2$}(ClO$_4$)$_2$ [1b](ClO$_4$)$_2$. The precursor complex [Cl_3Ru^{III}(μ-tppz)$Ru^{III}Cl_3$] (100 mg, 0.124 mmol) and the ligand BIAN (R = H = (bis(phenyl)-acenaphthenequinonediimine) (82 mg, 0.248 mmol) were mixed in 30 mL of ethanol, and the mixture was heated to reflux for 16 h under dinitrogen atmosphere. The color of the initially greenish solution gradually changed to deep green. The reaction mixture was evaporated to dryness under reduced pressure. The resulting solid mass was dissolved in a minimum volume of acetonitrile, followed by addition of a saturated aqueous solution of sodium perchlorate to yield a dark green precipitate, which was filtered and washed thoroughly by ice water and dried in vacuo. The product was purified using a silica gel (mesh 60−120) column. The deep green dinuclear complex [**1b**]$(ClO_4)_2$ was eluted by a solvent mixture of CH_2Cl_2−CH_3CN (2:1). Evaporation of solvent under reduced pressure yielded pure [**1b**]$(ClO_4)_2$.

dx.doi.org/10.1021/ic500730m | *Inorg. Chem.* 2014, 53, 7389−7403

[1b](ClO4)2. Yield, 114 mg (60%). ^{1}H NMR in CD_3CN [δ/ppm (*J*/Hz)]: 8.81 (d, 7.9, 1H), 8.72 (d, 5.2, 2H), 8.22 (d, 8.3, 2H), 8.12 (d, 8.2, 1H), 8.08 (t, 7.8, 8.0, 3H), 8.01 (m, 1H), 7.80 (b, 3H), 7.72 (m, 3H), 7.49 (d, 7.3, 1H), 7.39 (t, 7.5, 8.0, 1H), 7.07 (m, 1H), 6.81 (t, 5.02, 5.05, 1H), 6.73 (t, 7.5, 7.6, 1H), 6.69 (d, 7.4, 1H), 6.33 (d, 7.3, 1H), 5.09 (d, 7.1, 1H). MS (ESI+, CH_3CN): *m*/*z* {[[**1b**]$(ClO_4)_2$-$ClO_4]^+$} calcd: 1425.72; found: 1425.43. IR (KBr): ν (ClO_4^-, cm^{-1}): 1089, 626. Molar conductivity (CH_3CN): Λ_M = 205 Ω^{-1} cm^2 M^{-1}. Anal. Calcd for $C_{72}H_{48}Cl_4N_{10}O_8Ru_2$: C, 56.70; H, 3.17; N, 9.18; found: C, 56.57; H, 3.19; N, 9.31%.

[2b](ClO4)2. Yield, 125 mg (63%). ^{1}H NMR in CD_3CN [δ/ppm (*J*/Hz)]: 8.81 (d, 7.8, 1H), 8.65 (d, 20, 2H), 8.14 (d, 8.4, 1H), 8.04 (m, 4H), 7.89 (d, 17.92, 2H), 7.64 (m, 3H), 7.55 (b, 2H), 7.50 (d, 7.3, 1H), 7.32 (t, 8.0, 7.50, 1H), 6.81 (d, 7.00, 1H), 6.72 (d, 7.2, 1H), 6.49 (d, 7.5, 1H), 6.14 (d, 7.00, 1H), 4.84 (d, 6.9, 1H), 2.61 (s, 3H, BIAN), 1.57 (s, 3H, BIAN). MS (ESI+, CH_3CN): *m*/*z* {[[**2b**]$(ClO_4)_2$-$ClO_4]^+$} calcd: 1481.82; found: 1481.72. IR (KBr): ν (ClO_4^-, cm^{-1}): 1092, 623. Molar conductivity (CH_3CN): Λ_M = 210 Ω^{-1} cm^2 M^{-1}. Anal. Calcd for $C_{76}H_{56}Cl_4N_{10}O_8Ru_2$: C, 57.73; H, 3.57; N, 8.86; found: C, 57.60; H, 3.45; N, 8.68%.

[3b](ClO4)2. Yield, 134 mg (65%). ^{1}H NMR in CD_3CN [δ/ppm (*J*/Hz)]: 8.89 (d, 7.92, 1H), 8.70 (d, 15.76, 2H), 8.21 (d, 8.3, 1H), 8.07 (m, 6H), 7.71 (m, 3H), 7.64 (d, 7.3, 1H), 7.40 (t, 7.8, 7.6, 1H), 7.33 (d, 7.2, 2H), 6.82 (d, 7.2, 1H), 6.61 (d, 7.9, 1H), 6.30 (m, 2H), 5.10 (d, 7.9, 1H), 4.06 (s, 3H, BIAN), 3.22 (s, 3H, BIAN). MS (ESI+, CH_3CN): *m*/*z* {[[**3b**]$(ClO_4)_2$-$ClO_4]^+$} calcd: 1545.82; found: 1545.71. IR (KBr): ν (ClO_4^-, cm^{-1}): 1093, 622. Molar conductivity (CH_3CN): Λ_M = 213 Ω^{-1} cm^2 M^{-1}. Anal. Calcd for $C_{76}H_{56}Cl_4N_{10}O_{12}Ru_2$: C, 55.48; H, 3.43; N, 8.51; found: C, 55.35; H, 3.40; N, 8.65%.

[4b](ClO4)2. Yield, 119 mg (57%). ^{1}H NMR in CD_3CN [δ/ppm (*J*/Hz)]: 8.85 (d, 8.1, 1H), 8.70 (d, 5.9, 1H), 8.64 (d, 5.50, 1H) 8.25 (d, 8.2, 1H), 8.14 (d, 7.7, 2H), 8.05 (d, 6.6, 4H), 7.80 (b, 2H), 7.75 (t, 7.4, 8.2, 3H), 7.65 (d, 7.2, 1H), 7.42 (t, 7.4, 8.2, 1H), 7.12 (d, 8.0, 1H), 6.83 (d, 7.2, 1H), 6.78 (d, 8.2, 1H), 6.37 (d, 7.8, 1H), 5.14 (d, 7.2, 1H). MS (ESI+, CH_3CN): *m*/*z* {[[**4b**]$(ClO_4)_2$-$ClO_4]^+$} calcd: 1563.49; found: 1563.50. IR (KBr): ν (ClO_4^-, cm^{-1}): 1091, 624. Molar conductivity (CH_3CN): Λ_M = 220 Ω^{-1} cm^2 M^{-1}. Anal. Calcd for $C_{72}H_{44}Cl_8N_{10}O_8Ru_2$: C, 52.00; H, 2.67; N, 8.42; found: C, 52.25; H, 2.65; N, 8.54%.

■ ASSOCIATED CONTENT

Ⓢ Supporting Information

X-ray crystallographic files in CIF format for BIAN (R = Me) (CCDC No. 994206), **1a** (CCDC No. 994200), **2a** (CCDC No. 994201), **4a** (CCDC No. 994202), **5a** (CCDC No. 994203), [**2b**]$(ClO_4)_2$ (CCDC No. 994204), [**3b**]$(ClO_4)_2$ (CCDC No. 994205), crystal data (Figures S1−S4, Tables S1, S2, S5, S6 and S18), mass spectra (Figures S13 and S20), ^{1}H NMR (Figures S14 and S21), DFT data set for **1a**^{n}, **5a**^{n}, and **2b**^{n} (Figures S5−S7, S15, Tables S3, S4, S7−S17, S19−S26), UV−vis−NIR data (Figures S8, S9, S16−S18, Table S27), EPR data (Figures S10−S12, S19). This material is available free of charge via the Internet at http://pubs.acs.org.

■ AUTHOR INFORMATION

Corresponding Authors

*E-mail: lahiri@chem.iitb.ac.in. Phone: +91 22 25767159. Fax: +91 22 25723480. (G.K.L.)

*E-mail: kaim@iac.uni-stuttgart.de. Phone: +49(0)711/685-64170. Fax: +49(0)711/685−64165. (W.K.)

Notes

The authors declare no competing financial interest.

■ ACKNOWLEDGMENTS

Financial support received from the Department of Science and Technology and the Council of Scientific and Industrial Research (fellowship to P.M. and H.A.), New Delhi (India), the DAAD, FCI, and DFG (Germany), is gratefully acknowledged.

■ REFERENCES

(1) (a) van Asselt, R.; Elsevier, C. J.; Smeets, W. J. J.; Spek, A. L. *Inorg. Chem.* **1994**, *33*, 1521. (b) Scarel, A.; Axet, M. R.; Amoroso, F.; Ragaini, F.; Elsevier, C. J.; Holuigue, A.; Carfagna, C.; Mosca, L.; Milani, B. *Organometallics* **2008**, *27*, 1486. (c) Kooijman, H.; Spek, A. L.; van Belzen, R.; Elsevier, C. J. *Acta Crystallogr., Sect. C: Cryst. Struct. Commun.* **1997**, *53*, 1593. (d) Groen, J. H.; de Jong, B. J.; Ernsting, J.-M.; van Leeuwen, P.W. N. M.; Vrieze, K.; Smeets, W. J. J.; Spek, A. L. *J. Organomet. Chem.* **1999**, *573*, 3.

(2) Hill, N. J.; Baca, I. V.; Cowley, A. H. *Dalton Trans.* **2009**, 240.

(3) Ragaini, F.; Cenini, S.; Borsani, E.; Dompe, M.; Gallo, E. *Organometallics* **2001**, *20*, 3393.

(4) (a) Fedushkin, I. L.; Skatova, A. A.; Chudakova, V. A.; Fukin, G. K. *Angew. Chem., Int. Ed.* **2003**, *42*, 3294. (b) Fedushkin, I. L.; Skatova, A. A.; Chudakova, V. A.; Cherkasov, V. K.; Fukin, G. K.; Lopatin, M. A. *Eur. J. Inorg. Chem.* **2004**, 388. (c) Fedushkin, I. L.; Markina, O. V.; Lukoyanov, A. N.; Morozov, A. G.; Baranov, E. V.; Maslov, M. O.; Ketkov, S. Y. *Dalton Trans.* **2013**, *42*, 7952.

(5) Fedushkin, I. L.; Maslova, O. V.; Morozov, A. G.; Dechert, S.; Demeshko, S.; Meyer, F. *Angew. Chem., Int. Ed.* **2012**, *51*, 1.

(6) Clark, M. K.; Bendix, J.; Heyduk, A. F.; Ziller, J. W. *Inorg. Chem.* **2012**, *51*, 7457.

(7) (a) Li, L.; Lopes, P. S.; Rosa, V.; Figueira, C. A.; Lemos, M. A. N. D. A.; Duarte, M. T.; Avilés, T.; Gomes, P. T. *Dalton Trans.* **2012**, *41*, 5144. (b) Singh, S. K.; Dubey, S. K.; Pandey, R.; Mishra, L.; Zou, R.-Q.; Xu, Q.; Pandey, D. S. *Polyhedron* **2008**, *27*, 2877. (c) Shiotsuki, M.; White, P. S.; Brookhart, M.; Templeton, V. *J. Am. Chem. Soc.* **2007**, *129*, 4058. (d) Papanikolaou, P. A.; Gdaniec, M.; Wicher, B.; Akrivos, P. D.; Tkachenko, N. V. *Eur. J. Inorg. Chem.* **2013**, 5196. (e) Vigan, M.; Ragaini, F.; Buonomenna, M. G.; Lariccia, R.; Caselli, A.; Gallo, E.; Cenini, S.; Jansen, J. C.; Drioli, E. *ChemCatChem* **2010**, *2*, 1150.

(8) Kaim, W. *J. Am. Chem. Soc.* **1982**, *104*, 3833.

(9) (a) Friedman, A. E.; Chambron, J. C.; Sauvage, J. P.; Turro, N. J.; Barton, J. K. *J. Am. Chem. Soc.* **1990**, *112*, 4960. (b) Fees, J.; Kaim, W.; Moscherosch, M.; Matheis, W.; Klima, J.; Krejcik, M.; Záliš, S. *Inorg. Chem.* **1993**, *32*, 166.

(10) (a) Bulak, E.; Varnali, T.; Schwederski, B.; Sarkar, B.; Hartenbach, I.; Fiedler, J.; Kaim, W. *Dalton Trans.* **2011**, *40*, 2757. (b) Bulak, E.; Varnali, T.; Schwederski, B.; Bubrin, D.; Fiedler, J.; Kaim, W. *Organometallics* **2011**, *30*, 6441.

(11) Waldhör, E.; Zulu, M. M.; Záliš, S.; Kaim, W. *J. Chem. Soc., Perkin Trans. 2* **1996**, 1197.

(12) (a) Roy, S.; Sarkar, B.; Imrich, H.-G.; Fiedler, J.; Záliš, S.; Jiménez-Aparicio, R.; Urbanos, F. A.; Mobin, S. M.; Lahiri, G. K.; Kaim, W. *Inorg. Chem.* **2012**, *51*, 9273. (b) Das, A.; Scherer, T.; Maji, S.; Mondal, T. K.; Mobin, S. M.; Urbanos, F. A.; Jiménez-Aparicio, R.; Kaim, W.; Lahiri, G. K. *Inorg. Chem.* **2011**, *50*, 7040. (c) Kundu, T.; Mobin, S. M.; Lahiri, G. K. *Dalton Trans.* **2010**, *39*, 4471. (d) Kumbhakar, D.; Sarkar, B.; Maji, S.; Mobin, S. M.; Fiedler, J.; Urbanos, F. A.; Jiménez-Aparicio, R.; Kaim, W.; Lahiri, G. K. *J. Am. Chem. Soc.* **2008**, *130*, 17575. (e) Maji, S.; Sarkar, B.; Mobin, S. M.; Fiedler, J.; Urbanos, F. A.; Jiménez-Aparicio, R.; Kaim, W.; Lahiri, G. K. *Inorg. Chem.* **2008**, *47*, 5204. (f) Agarwala, H.; Scherer, T.; Maji, S.; Mondal, T. K.; Mobin, S. M.; Fiedler, J.; Urbanos, F. A.; Jiménez-Aparicio, R.; Kaim, W.; Lahiri, G. K. *Chem.—Eur. J.* **2012**, *18*, 5667. (g) Kar, S.; Sarkar, B.; Ghumaan, S.; Roy, D.; Urbanos, F. A.; Fiedler, J.; Sunoj, R. B.; Jiménez-Aparicio, R.; Kaim, W.; Lahiri, G. K. *Inorg. Chem.* **2005**, *44*, 8715. (h) Hoshino, Y.; Higuchi, S.; Fiedler, J.; Su, C.-Y.; Knödler, A.; Schwederski, B.; Sarkar, B.; Hartmann, H.; Kaim, W. *Angew. Chem.* **2003**, *115*, 698; *Angew. Chem., Int. Ed.* **2003**, *42*, 674.

(13) (a) Kundu, T.; Sarkar, B.; Mondal, T. K.; Fiedler, J.; Mobin, S. M.; Kaim, W.; Lahiri, G. K. *Inorg. Chem.* **2010**, *49*, 6565. (b) Kundu, T.; Sarkar, B.; Mondal, T. K.; Mobin, S. M.; Urbanos, F. A.; Jiménez-Aparicio, R.; Fiedler, J.; Kaim, W.; Lahiri, G. K. *Inorg. Chem.* **2011**, *50*, 4753. (c) Das, A. K.; Sarkar, B.; Fiedler, J.; Záliš, S.; Hartenbach, I.; Strobel, S.; Lahiri, G. K.; Kaim, W. *J. Am. Chem. Soc.* **2009**, *131*, 8895.
(14) Kaim, W. *Inorg. Chem.* **2011**, *50*, 9752.
(15) Das, D.; Das, A. K.; Sarkar, B.; Mondal, T. K.; Mobin, S. M.; Fiedler, J.; Záliš, S.; Urbanos, F. A.; Jiménez-Aparicio, R.; Kaim, W.; Lahiri, G. K. *Inorg. Chem.* **2009**, *48*, 11853.
(16) Mandal, A.; Kundu, T.; Ehret, F.; Bubrin, M.; Mobin, S. M.; Kaim, W.; Lahiri, G. K. *Dalton Trans.* **2014**, *43*, 2473.
(17) Grupp, A.; Bubrin, M.; Ehret, F.; Zeng, Q.; Hartl, F.; Kvapilová, H.; Záliš, S.; Kaim, W. *Eur. J. Inorg. Chem.* **2014**, 110.
(18) Kalinina, D.; Dares, C.; Kaluarachchi, H.; Potvin, P. G.; Lever, A. B. P. *Inorg. Chem.* **2008**, *47*, 10110.
(19) Bowman, A. C.; England, J.; Sproules, S.; Weyhermüller, T.; Wieghardt, K. *Inorg. Chem.* **2013**, *52*, 2242.
(20) (a) Muresan, N.; Weyhermüller, T.; Wieghardt, K. *Dalton Trans.* **2007**, 4390. (b) Khusniyarov, M. M.; Weyhermüller, T.; Bill, E.; Wieghardt, K. *Angew. Chem.* **2008**, *120*, 1248; *Angew. Chem., Int. Ed.* **2008**, *47*, 1228. (c) Brown, S. N. *Inorg. Chem.* **2012**, *51*, 1251.
(21) (a) Grupp, A.; Bubrin, M.; Ehret, F.; Kvapilová, H.; Záliš, S.; Kaim, W. *J. Organomet. Chem.* **2014**, *751*, 678. (b) Drozdz, A.; Bubrin, M.; Fiedler, J.; Záliš, S.; Kaim, W. *Dalton Trans.* **2012**, *41*, 1013. (c) Löw, I.; Bubrin, M.; Paretzki, A.; Fiedler, J.; Zalis, S.; Kaim, W., unpublished results.
(22) (a) Coventry, D. N.; Batsanov, A. S.; Goeta, A. E.; Howard, J. A. K.; Marder, T. B. *Polyhedron* **2004**, *23*, 2789. (b) El-Ayaan, U.; Murata, F.; El-Derby, S.; Fukuda, Y. *J. Mol. Struct.* **2004**, *692*, 209.
(23) (a) Roy, S.; Sieger, M.; Sarkar, B.; Schwederski, B.; Lissner, F.; Schleid, Th.; Fiedler, J.; Kaim, W. *Angew. Chem.* **2008**, *120*, 6287; *Angew. Chem., Int. Ed.* **2008**, *47*, 6192. (b) Ehret, F.; Bubrin, M.; Hübner, R.; Schweinfurth, D.; Hartenbach, I.; Záliš, S.; Kaim, W. *Inorg. Chem.* **2012**, *51*, 6237.
(24) (a) Sarkar, B.; Patra, S.; Fiedler, J.; Sunoj, R. B.; Janardanan, D.; Mobin, S. M.; Niemeyer, M.; Lahiri, G. K.; Kaim, W. *Angew. Chem.* **2005**, *117*, 5800; *Angew. Chem., Int. Ed.* **2005**, *44*, 5655. (b) Sarkar, B.; Patra, S.; Fiedler, J.; Sunoj, R. B.; Janardanan, D.; Lahiri, G. K.; Kaim, W. *J. Am. Chem. Soc.* **2008**, *130*, 3532.
(25) Corn, I. R.; Astudillo-Sanchez, P. D.; Zdilla, M. J.; Fanwick, P. E.; Shaw, M. J.; Miller, J. T.; Evans, D. H.; Abu-Omar, M. M. *Inorg. Chem.* **2013**, *52*, 5457.
(26) (a) Patra, S.; Sarkar, B.; Mobin, S. M.; Kaim, W.; Lahiri, G. K. *Inorg. Chem.* **2003**, *42*, 6469. (b) Kaim, W.; Ernst, S.; Kasack, V. *J. Am. Chem. Soc.* **1990**, *112*, 173.
(27) Kaim, W.; Lahiri, G. K. *Angew. Chem.* **2007**, *119*, 1808; *Angew. Chem., Int. Ed.* **2007**, *46*, 1778.
(28) Kaim, W. *Angew. Chem.* **1983**, *95*, 201; *Angew. Chem., Int. Ed. Engl.* **1983**, *22*, 171.
(29) Scheiring, T.; Kaim, W.; Olabe, J. A.; Parise, A. R.; Fiedler, J. *Inorg. Chim. Acta* **2000**, *300*−*302*, 125.
(30) Chanda, N.; Laye, R. H.; Chakraborty, S.; Paul, R. L.; Jeffery, J. C.; Ward, M. D.; Lahiri, G. K. *J. Chem. Soc., Dalton Trans.* **2002**, 3496.
(31) Kundu, T.; Schweinfurth, D.; Sarkar, B.; Mondal, T. K.; Fiedler, J.; Mobin, S. M.; Puranik, V. G.; Kaim, W.; Lahiri, G. K. *Dalton Trans.* **2012**, *41*, 13429.
(32) Robin, M. B.; Day, P. *Adv. Inorg. Chem. Radiochem.* **1967**, *10*, 247.
(33) Creutz, C. *Prog. Inorg. Chem.* **1983**, *30*, 1.
(34) (a) Kobayashi, T.; Nishina, Y.; Shimizu, K. G.; Satô, G. P. *Chem. Lett.* **1988**, 1137. (b) Kasahara, Y.; Hoshino, Y.; Shimizu, K.; Sato, G. P. *Chem. Lett.* **1990**, 381.
(35) Hartshorn, C. M.; Daire, N.; Tondreau, V.; Loeb, B.; Meyer, T. J.; White, P. S. *Inorg. Chem.* **1999**, *38*, 3200.
(36) Mak, C. S. K.; Wong, H. L.; Leung, Q. Y.; Tam, W. Y.; Chan, W. K.; Djurišic, A. B. *J. Organomet. Chem.* **2009**, *694*, 2770.
(37) Krejčik, M.; Danek, M.; Hartl, F. *J. Electroanal. Chem. Interfacial Electrochem.* **1991**, *317*, 179.
(38) (a) Sheldrick, G. M. *Acta Crystallogr., Sect. A* **2008**, *A64*, 112. (b) *Program for Crystal Structure Solution and Refinement;* University of Goettingen: Goettingen, Germany, 1997.
(39) Lee, C.; Yang, W.; Parr, R. G. *Phys. Rev. B* **1988**, *37*, 785.
(40) (a) Andrae, D.; Haeussermann, U.; Dolg, M.; Stoll, H.; Preuss, H. *Theor. Chim. Acta.* **1990**, *77*, 123. (b) Fuentealba, P.; Preuss, H.; Stoll, H.; Szentpaly, L. V. *Chem. Phys. Lett.* **1989**, *89*, 418.
(41) Frisch, M. J.; Trucks, G. W.; Schlegel, H. B.; Scuseria, G. E.; Robb, M. A.; Cheeseman, J. R.; Scalmani, G.; Barone, V.; Mennucci, B.; Petersson, G. A.; Nakatsuji, H.; Caricato, M.; Li, X.; Hratchian, H. P.; Izmaylov, A. F.; Bloino, J.; Zheng, G.; Sonnenberg, J. L.; Hada, M.; Ehara, M.; Toyota, K.; Fukuda, R.; Hasegawa, J.; Ishida, M.; Nakajima, T.; Honda, Y.; Kitao, O.; Nakai, H.; Vreven, T.; Montgomery, J. A.; Peralta, Jr. J. E.; Ogliaro, F.; Bearpark, M.; Heyd, J. J.; Brothers, E.; Kudin, K. N.; Staroverov, V. N.; Kobayashi, R.; Normand, J.; Raghavachari, K.; Rendell, A.; Burant, J. C.; Iyengar, S. S.; Tomasi, J.; Cossi, M.; Rega, N.; Millam, J. M.; Klene, M.; Knox, J. E.; Cross, J. B.; Bakken, V.; Adamo, C.; Jaramillo, J.; Gomperts, R.; Stratmann, R. E.; Yazyev, O.; Austin, A. J.; Cammi, R.; Pomelli, C.; Ochterski, J. W.; Martin, R. L.; Morokuma, K.; Zakrzewski, V. G.; Voth, G. A.; Salvador, P.; Dannenberg, J. J.; Dapprich, S.; Daniels, A. D.; Farkas, O.; Foresman, J. B.; Ortiz, J. V.; Cioslowski, J.; Fox, D. J. *Gaussian 09 (Revision A.02);* Gaussian, Inc.: Wallingford, CT, 2009.
(42) (a) Bauernschmitt, R.; Ahlrichs, R. *Chem. Phys. Lett.* **1996**, *256*, 454. (b) Stratmann, R. E.; Scuseria, G. E.; Frisch, M. J. *J. Chem. Phys.* **1998**, *109*, 8218. (c) Casida, M. E.; Jamorski, C.; Casida, K. C.; Salahub, D. R. *J. Chem. Phys.* **1998**, *108*, 4439.
(43) (a) Barone, V.; Cossi, M. *J. Phys. Chem. A* **1998**, *102*, 1995. (b) Cossi, M.; Barone, V. *J. Chem. Phys.* **2001**, *115*, 4708. (c) Cossi, M.; Rega, N.; Scalmani, G.; Barone, V. *J. Comput. Chem.* **2003**, *24*, 669.
(44) Leonid, S. Chemissian 1.7. 2005−2010. http://www.chemissian.com.
(45) Zhurko, D. A.; Zhurko, G. A. ChemCraft 1.5; Plimus: San Diego, CA. http://www.chemcraftprog.com.